Geochronology and isotope analysis of the Late Paleozoic to Mesozoic granitoids from northeastern Vietnam and implications for the evolution of the South China block

- Zechao Chen[a, e]
- Wei Lin[a]
- Michel Faure[b]
- Claude Lepvrier[c]
- Nguyen Van Vuong[d]
- Vu Van Tich[d]

- [a] State Key Laboratory of Lithospheric Evolution, Institute of Geology and Geophysics, Chinese Academy of Sciences, Beijing, China
- [b] Institut des Sciences de la Terre d'Orléans (ISTO), UMR CNRS 6113, Université d'Orléans, 45067 Orléans Cedex 2, France
- [c] Institut des Sciences de la Terre de Paris (ISTeP), UMR CNRS 7193, Case 129, Université Pierre & Marie Curie, 4 Place Jussieu, 75252 Paris Cedex 05, France
- [d] Faculty of Geology, Hanoi University of Science, 334 Nguyen Trai, Thanh Xuan, Hanoi, Viet Nam
- [e] Graduate University of Chinese Academy of Sciences, Beijing 100049, China

Abstract

In northeastern Vietnam, Late Paleozoic and Permo-Triassic granitic plutons are widespread, but their tectonic significance is controversial. In order to understand the regional magmatism and crustal evolution processes of the South China block (SCB), this study reports integrated in situ U–Pb, Hf–O and Sr–Nd isotope analyses of granitic rocks from five plutons in northeastern Vietnam. Zircon SIMS U–Pb ages of six granitic samples cluster around in two groups 255–228 Ma and 90 Ma. Bulk-rock ε_{Nd} (t) ranges from −11 to −9.7, suggesting that continental crust materials were involved in their granitic genesis. In situ zircon Hf–O isotopic measurements for the granitic samples yield a mixing trend between the mantle- and supracrustal-derived melts. It is suggested that the granitic rocks were formed by re-melting of the continental crust. These new data are compared with the Paleozoic and Mesozoic granitic rocks of South China. We argue that northeastern Vietnam belongs to the South China block. Though still speculated, an ophiolitic suture between NE Vietnam and South China, so-called Babu ophiolite, appears unlikely. The Late Paleozoic to Mesozoic magmatism in the research area provides new insights for the magmatic evolution of the South China block.

Keywords : Northeastern Vietnam; South China block; Triassic orogen; Zircon SIMS dating; Hf–O isotopes; Eastern Paleotethys

1. Introduction

Southeastern Eurasia is an important part of the tectonic framework in the continental margin of eastern Asia and it was considered as the result of collision or accretion processes by several micro-continents with the South China block (SCB) during Permian-Triassic ca. 270–240 Ma (Nagy et al., 2001, Osanai et al., 2001, Osanai et al., 2006, Lan et al., 2003, Nakano et al., 2008, Lepvrier et al., 2008 and Sone and Metcalfe, 2008). As one of the largest blocks on southeastern Eurasia, the SCB is composed of the Yangtze craton to the northwest and the Cathaysia block in the southeast, respectively (Shui, 1987, Yu et al., 2006, Yu et al., 2007 and Wang et al., 2012a). These two blocks were welded together during the Neoproterozoic Jiangnan collision formed at ca. 970–820 Ma (Huang, 1978, Zhang et al., 1984, Shu et al., 1994, Li, 1999, Wu et al., 2006b and Li et al., 2009a, and references therein). The Jiangshan-Shaoxing Fault represents the ophiolitic suture between the Yangtze and Cathaysia blocks (Zhou and Zhu, 1993 and Shu et al., 2008b). From the Late Neoproterozoic to the late Early Paleozoic, the SCB underwent a continuous sedimentation, partly controlled by rifting until the Late Ordovician (Wang and Li, 2003). Since Silurian, the SCB experienced several tectono-thermal events during Late Silurian-Early Devonian, Late Permian-Triassic and Late Mesozoic in different regions (Chen, 1999, Zhou and Li, 2000, Wang et al., 2005, Zhou et al., 2006, Li and Li, 2007, Liang et al., 2008, Faure et al., 2009 and Chu and Lin, this volume). The Late Silurian-Early Devonian event is sealed by a Middle Devonian angular unconformity and the intrusion of Silurian granitoids in the southern part of South China (Huang et al., 1980, JBGMR, 1984, HBGMR, 1988, Yan et al., 2006, Wang et al., 2007c and Wang et al., 2011). The Early Paleozoic orogenic belt is well developed south of the Jiangshan-Shaoxing Fault (Wang et al., 2007c, Faure et al., 2009, Li et al., 2010d and Charvet et al., 2010). It is an intracontinental orogenic belt characterized by south-directed structures, followed by syn- to post- tectonic crustal melting (Lin et al., 2008 and Faure et al., 2009).

The most important tectonic event experienced by the SCB took place in the Early Mesozoic, as recognized by a Late Triassic unconformity widespread across the SCB (Huang et al., 1980, GXBGMR, 1982, JBGMR, 1984 and HBGMR, 1988). Permian-Triassic orogenic belts are well developed around the block, such as Qinling-Dabieshan-Sulu (Hacker et al., 1998, Faure et al., 1999 and Leech and Webb, 2012 and references therein), Songpan-Ganzi (Roger et al., 2010 and Yan et al., 2011), Sanjiang Tethyan (Jian et al., 1999, Wang et al., 2000 and Hou et al., 2007 and reference therein), NE Vietnam (Lepvrier et al., 2011). The Jurassic and Cretaceous tectonic events in the SCB are expressed by granitic intrusions, acidic and intermediate volcanism, NE-SW trending normal or strike-slip faults, over-thrusts, extensional doming, and syn-tectonic terrigeneous sedimentation (Xu et al., 1987, Gilder et al., 1991, Faure et al., 1996, Lin et al., 2000, Wang et al., 2001, Li et al., 2001, Yan et al., 2003, Zhou et al., 2006 and Shu et al., 2008a). These Late Mesozoic tectonics were interpreted as the result of the subduction of a Paleo-Pacific oceanic plate beneath the Eurasia continent (John et al., 1990, Charvet et al., 1994, Faure et al., 1996, Zhou et al., 2006 and Li and Li, 2007Jahn). Geochemical studies of the Mesozoic mafic rocks east of the Xuefengshan fault suggest a continental rifting or intracontinental lithospheric extension in response to an upwelling of asthenosphere around 170 Ma (Li et al., 2004). However, the compressional deformation events during the Late Triassic to Middle Jurassic within the Cathaysia block (Charvet et al., 1994 and Chen, 1999) and Late Jurassic to Cretaceous within the southeastern part of Yangtze craton (Yan et al., 2003) make this interpretation unlikely. Therefore the Late Mesozoic tectonic evolution of the SCB is still controversial.

Granitoids occupy more than half of the surface of the southeastern part of the SCB (Fig. 1. GDBGMR, 1982, JBGMR, 1984, FBGMR, 1985, HBGMR, 1988 and ZBGMR, 1989). In order to understand the tectonic significance of these granitoids, many geochronological and geochemical works have been realized on these granitic rocks (Zhou and Li, 2000, Li et al., 2006, Wang et al., 2007b, Wang et al., 2007c, Li and Li, 2007 and Zhao et al., 2010; Cheng and Mao, 2010 and Chen et al., 2011). The Early Paleozoic granitoids are mostly distributed along Wuyi-Yunkai-Songchay massifs (JBGMR, 1984 and HBGMR, 1988). These plutons can be subdivided into gneissic and massive massifs defined on the basis of presence or absence of a well-developed magmatic fabric (JBGMR, 1984; HBGMR, 1988; Roger et al., 2000 and Wang et al., 2011). Available data show the age of these granitoids mostly range around 460–420 Ma with a per-aluminous character (Charvet et al., 2010, Wan et al., 2010, Li et al., 2010d, Wang et al., 2011 and Wang et al., 2012b). The Late Permian to Triassic granitoids mostly crop out in the Wuyi-Yunkai, Xuefengshan, Darongshan, and southern margin of SCB (Hainan island and NE Vietnam; Fig. 1; Zhou et al., 2006 and Li and Li, 2007). Previous studies of Late Permian-Triassic granitoids in the SCB indicated the majority of these granites has been classified as per-aluminous, and defined as S-type granites containing aluminous rich minerals such as muscovite, garnet and tourmaline (Chen and Jahn, 1998, Wang et al., 2002, Deng et al., 2004, Wang et al., 2005, Zhou et al., 2006, Wang et al., 2007b, Sun et al., 2004, Zhou et al., 2006 and Wang et al., 2007c, and references therein). The other plutons are Permian calc-alkaline *I*-type granite cropping out in Hainan Island (Li et al., 2006 and Li and Li, 2007, and references therein), and *A*-type granites (Sun et al., 2011). The Jurassic and Early Cretaceous granitoids are distributed at the eastern part of the SCB, along the Qinling-Dabieshan orogenic belt and Nanling belt (Fig. 1). Li and Li (2007) argue that these Jurassic to Early Cretaceous plutons correspond to synorogenic magmatism. They exhibit a younging trend toward the craton interior. Late Cretaceous granitic and volcanic rocks occupy most of the SE part of the SCB where they distribute parallel to the coastline (Fig. 1, Zhou and Li, 2000). The Late Mesozoic granitoids, synchronous mafic and ultramafic plutons constitute a bimodal magmatic association assumed to be controlled by lithospheric extension and asthenosphere upwelling within the eastern SCB (Chen and Zhu, 1993, Suo et al., 1999, Yan et al., 2006, Liang et al., 2008, Chen et al., 2008, Liu et al., 2010 and Wei et al., this volume). The origin of this magmatism is related to the Paleo-Pacific subduction (Wang et al., 2005 and Li and Li, 2007).

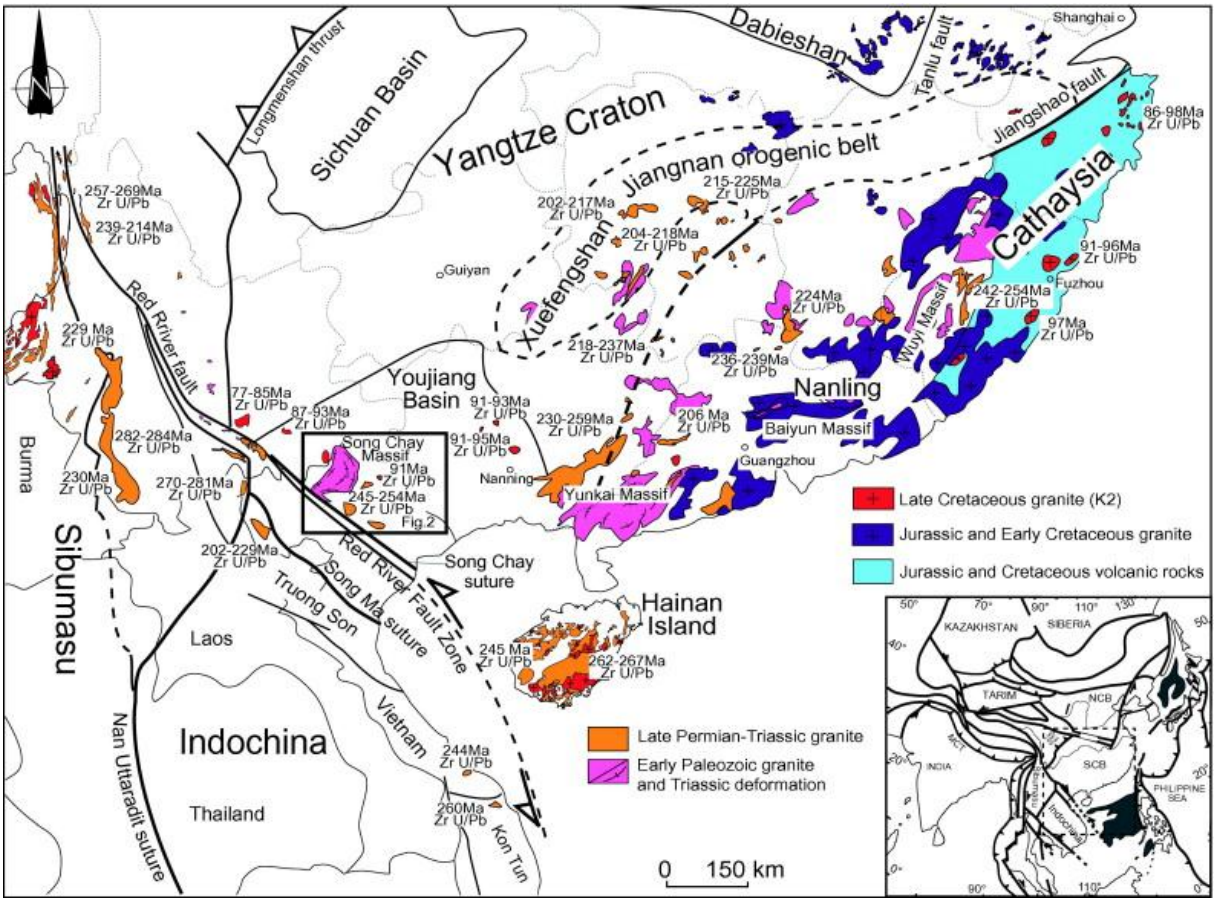

Fig. 1.

Geological map of South China and Indochina blocks, with the emphasis of the Paleozoic and Mesozoic magmatic rocks. Geochronological data from Li et al., 2006, Li, 1994, Li, 1999, Roger et al., 2000, Roger et al., 2012, Zhou and Li, 2000, Jian et al., 2003, Deng et al., 2004, Wang et al., 2005, Cai et al., 2006, Xie et al., 2006, Yan et al., 2006, Zhou et al., 2006, Li and Li, 2007, Liu et al., 2007, Wang et al., 2007a, Tran et al., 2008, Qiu et al., 2008, Tan et al., 2008 and Chen et al., 2009b; Chen et al., 2011, Liu et al., 2010, He et al., 2011 and Chu et al., 2012.

Granitic plutons are less abundant in the southwestern part of the SCB than in its eastern part. The majority of these plutons are dated of Late Permian to Triassic, and Late Cretaceous. In NE Vietnam, the works dealing with this Mesozoic plutonism are still rare (Fig. 2; Tran et al., 2008, Wang et al., 2011, Roger et al., 2000 and Roger et al., 2012), even though this area also belongs to the SCB (Lepvrier et al., 2011). Several questions arise, namely: (i) which tectonic event caused this granitic magmatism? (ii) are the NE Vietnam plutons comparable with those distributed in the eastern part of the SCB? This paper provides new SIMS U–Pb and isotopic data from different plutonic intrusions of NE Vietnam that will allow us to define the plutonic evolution of the southwestern margin of the SCB and discuss its tectonic significance.

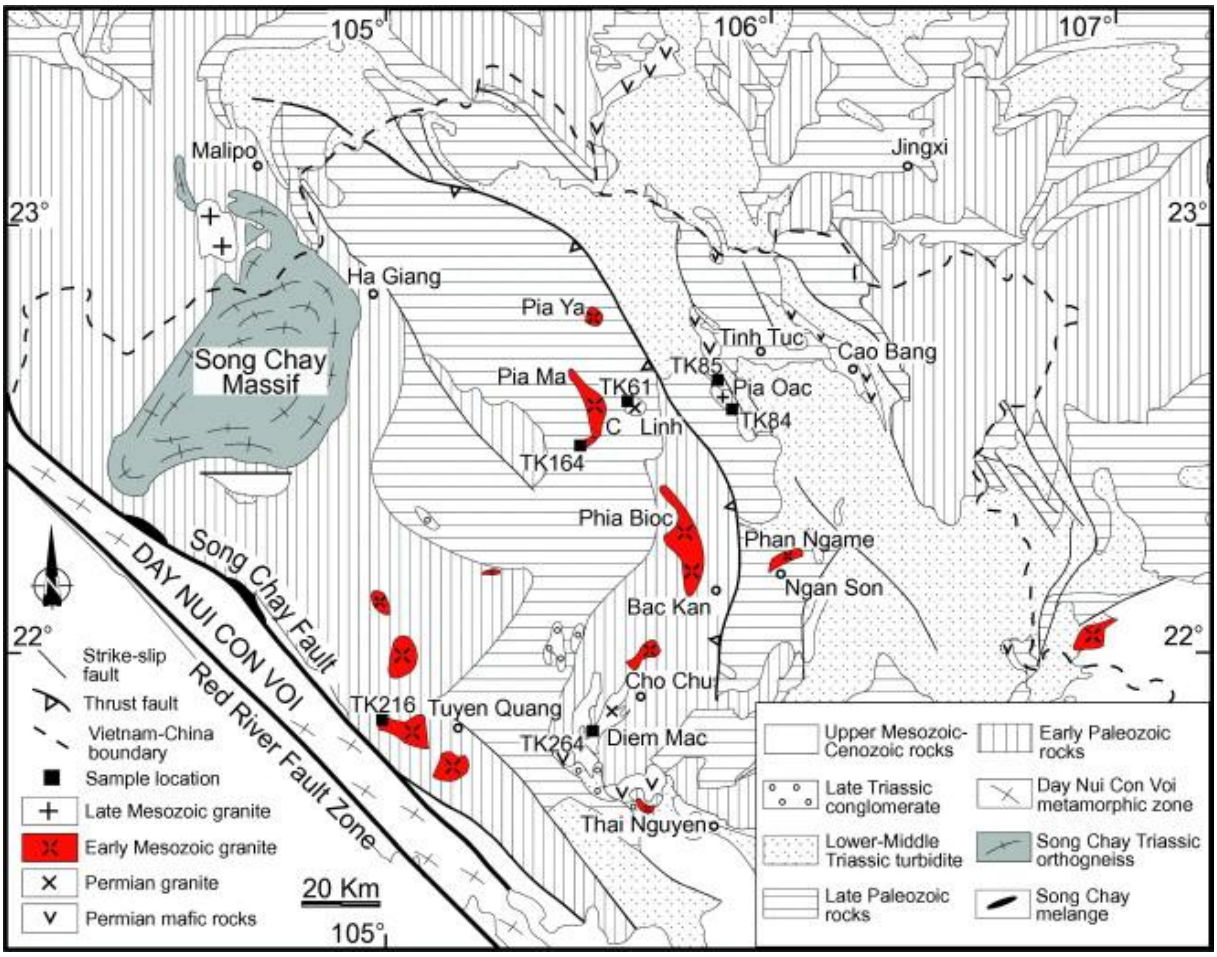

Fig. 2. : Simplified geologic map of northeastern Vietnam and adjacent area showing the locations of the dated sample.

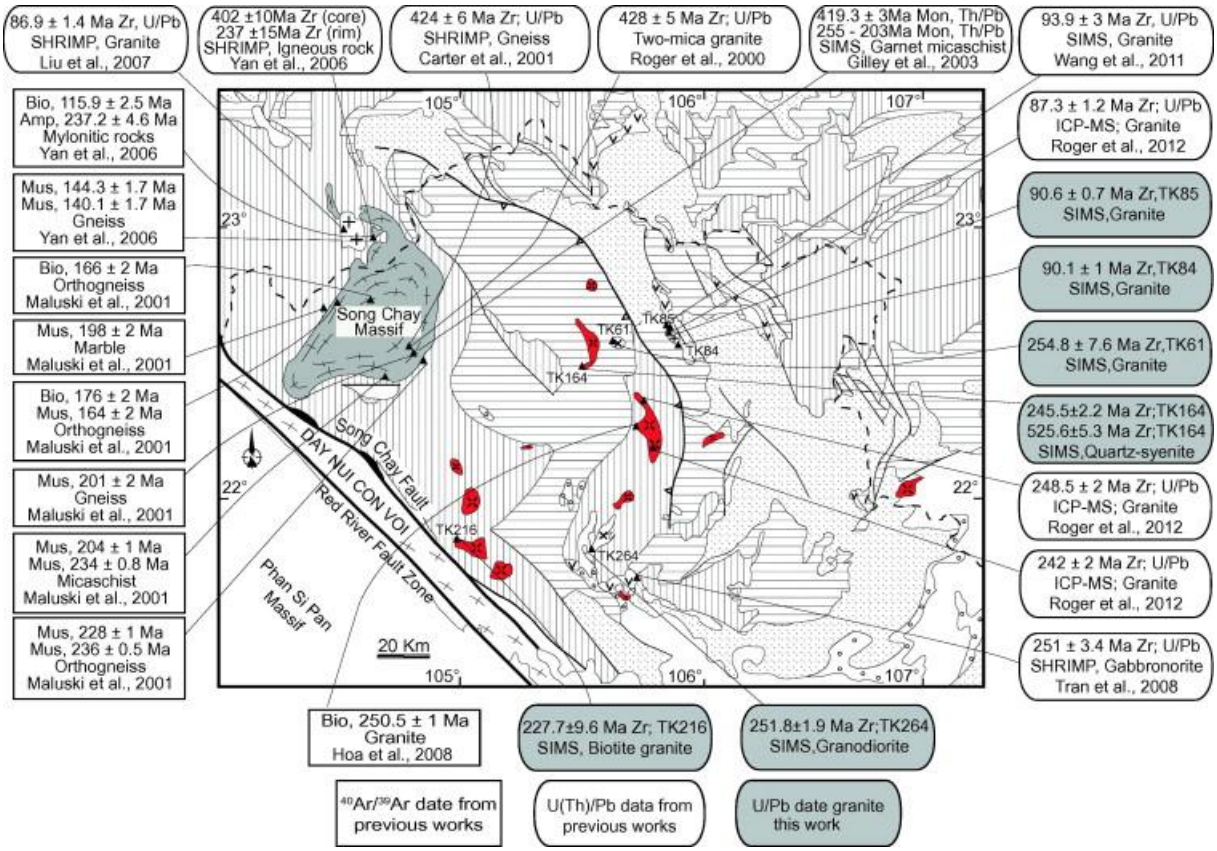

Fig. 3. : Map of the northern Vietnam and its adjacent area showing the available radiometric data. Six SIMS U/Pb ages of zircon are given in this paper. Symbols and captions in the map are the same as in Fig. 2.

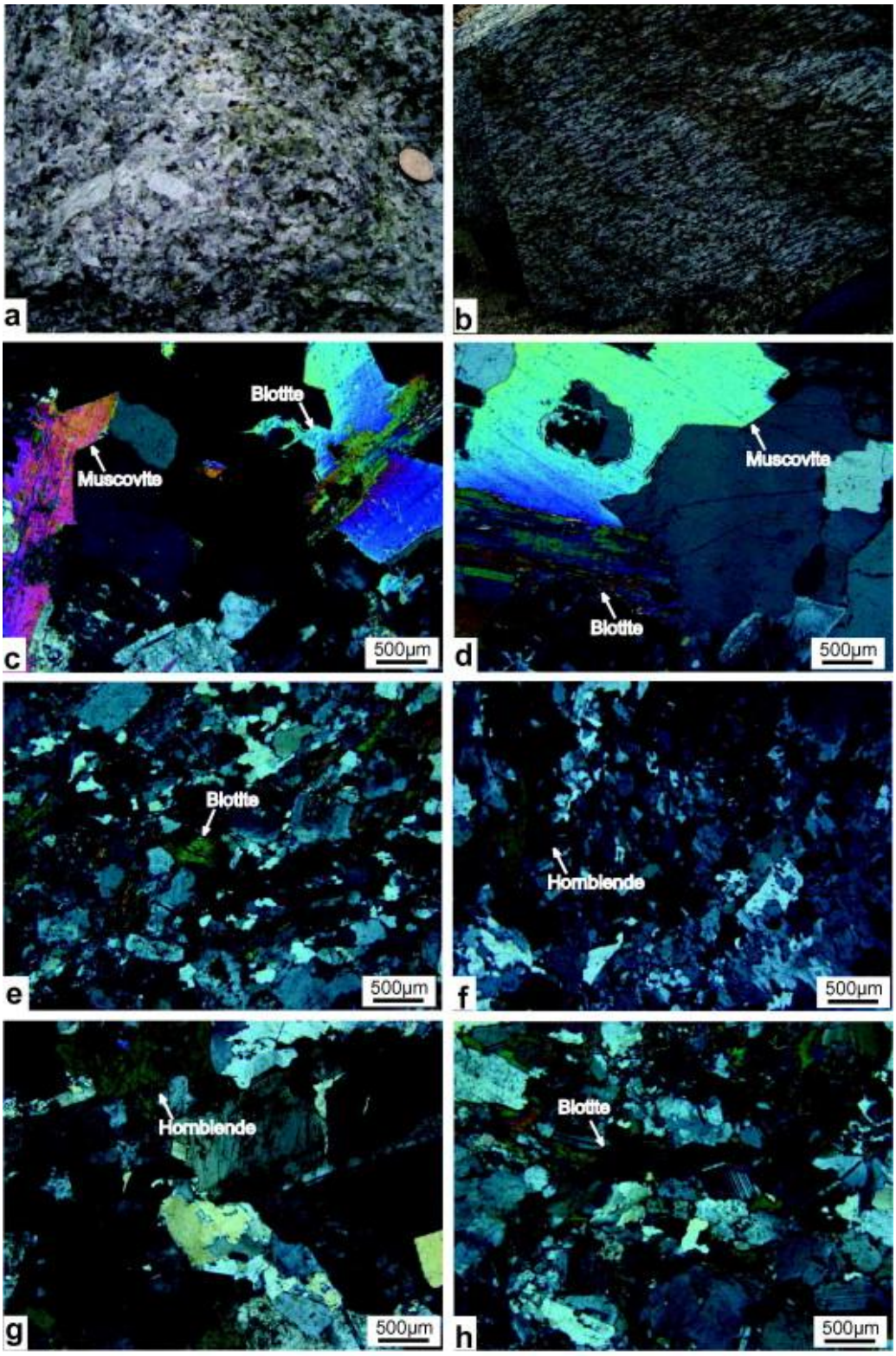

Fig. 4. : Photographs showing the character of granitic samples in northeastern Vietnam. (a) Leucogranites of Pia Oac pluton; (b) Pia Ma quartz-syenite foliated and lineated; (c) Microscope picture of sample TK84 two mica leucogranite; (d) Microscope picture of sample TK85 two mica leucogranite; (e) Microscope picture of sample TK216 biotite granite; f. Microscope picture of sample TK164 quartz-syenite; (g) Microscope picture of sample TK264 granodiorite; (h) Microscope picture of sample TK61 granodiorite.

2. Geological outline of the NE Vietnam

The southern boundary of the study area is the Red River Fault Zone (Fig. 2). This major left-lateral ductile shear zone with accommodated several hundreds of kilometers the southeastward during Oligo-Miocene extrusion of Sundaland and acted as a right-lateral fault from Late Pliocene (Tapponnier et al., 1990, Yang and Besse, 1993, Leloup et al., 1995 and Phan et al., 2012). The northern part of study area concerns Chinese Guangxi and Yunnan provinces where the stratigraphy is comparable with northeastern Vietnam (Fig. 2 and Table 1). In ascending stratigraphic order, six lithological and partly metamorphic series have been recognized, namely: (1) Neoproterozoic – Early Paleozoic terrigenous and carbonate sedimentary rocks, deposited in a shallow marine environment; (2) unmetamorphosed but strongly folded Devonian to Permian limestone, siliceous limestone, and some terrigenous rocks; (3) Lower to Middle Triassic turbiditic sediments (conglomerates, sandstones, tuffaceous sandstones, siltstones, shales) with rare carbonates; (4) Upper Triassic continental molassic formation that covers unconformably the previous series; (5) Late Mesozoic continental terrigenous red sandstone; (6) Cenozoic deposits in half-graben or rhombgraben basins along the Song Chay Fault (Fig. 2).

Table 1. : Stratigraphic column of study area.

Epoch	Litho unite	Thickness (m)	Deformation episode (Ma)	Tectonic regime	Intrusive Event	Tectonic interpretation
Quaternary	Pebble, granule, sand, silty clay	24–31				
Neogene	Conglomerate, gritstone, sandstone, Clay shale, coaly shale	600–800				
Paleogene	Conglomerate, sandstone, siltstone, Coaly shale, seams and lenses of lignite	959–2464		Extension		Regional extension in east Asia
Late Cretaceous	Conglomerate, gritstone, sandstone	200–300		Extension	Two-Mica Granite (91–90 Ma)	Regional extension?
Jurassic	Sandy siltstone, rhyolite, gritstone	1650–2000		Extension ?		Regional extension?
Late Triassic	Conglomerate, sandstone, clay shale, Coaly shale and coal	1200–1350	237–228 Ma		Biotite granite 227.7 ± 9.6 Ma	
Early-middle Triassic	Quartz porphyry and their tuffs, Sandy siltstone, conglomerate, clay shale	2040–2410		Thrusting	Quartz-syenite (245.5 ± 2.2 Ma)	Collision between Indochina and SCB
Permian	Thick bedded limestone, cherty shale	100–245			Granodiorite (255–251 Ma)	Subduction
Carboniferous	Limestone	350–600				
Devonian	Sandstone, shale, limestone	5680–6330				
Silurian	Mudstone, sandstone	400		?	Porphyritic granite (430–420 Ma)	Intracontinental Orogeny
Ordovician	Clayish limestone, quartzitic sandstone	2500–2600				
Cambrian	Shale, limestone	2000–2300			Quartz-syenite (525.6 ± 5.3 Ma)	

Paleozoic to Mesozoic granitic plutons intrude into the sedimentary succession (Fig. 2). The Song Chay massif that lies on the western part of the study area in northeastern Vietnam, is an augen-gneiss derived from a porphyritic monzogranite emplaced at 428 ± 5 Ma, according to U–Pb zircon age (Roger et al., 2000). The Phan Ngame orthogneiss that occupies the central part of the Ngan Son antiform (Bourret, 1922 and Fromaget, 1941) is equivalent to the Song Chay orthogneiss. It has been dated at 438.7 ± 3.5 Ma (Tran and Halpin, 2011). Furthermore, from north to south, there are several km-sized granitic plutons, namely the Pia Ya granitic pluton, Pia Ma quartz-syenite pluton, Cŏ Linh pluton, the Pia Oac leucocratic monzonite granite to the south of Tinh Tuc, the Phia Bioc massif locates in NW of Bac Kan (Fig. 2). Some granitic plutons outcrop along a NW-SE trend north of the Song Chay Fault (Fig. 2). The Phia Bioc granite is porphyritic and undeformed, containing microdioritic enclaves (Roger et al., 2012). This pluton cross-cuts Lower Triassic rocks but occurs as pebbles in the basal conglomerates of the Ladinian (242–235 Ma) sedimentary formation. It yields K–Ar ages scattered from 306 Ma to 230 Ma (Tri, 1979). Recently, this granitic pluton yielded zircon LA-ICPMS U–Pb ages scattered from 247 Ma to 242 Ma (Roger et al., 2012). The undeformed Pia Oac leucocratic monzonitic granite (Bourret, 1922), yields zircon U–Pb SIMS and LA-ICPMS ages of 94–87 Ma (Wang et al., 2011 and Roger et al., 2012). Alkaline mafic rocks that crop out near Cao Bang, west of Tinh Tuc and west of Thai Nguyen, are dated at 266–251 Ma (Tran et al., 2008). This Permian alkaline magmatism is regarded as being produced under the influence of the Emeishan mantle plume (Hanski et al., 2004 and Tran et al., 2008). The Late Permian to Triassic plutons were related to active continental margin magmatism (Liu et al., 2012) and intra-plate magmatism (Tran et al., 2008 and Roger et al., 2012), with the debates on the nature of subduction between SCB and Indochina blocks and suture zones (Lepvrier et al., 2008 and Lepvrier et al., 2011; Liu et al., 2012).

The boundary between the Indochina and South China blocks is generally considered to correspond to the Song Ma ophiolitic suture formed after a north directed subduction (Sengör et al., 1988, Metcalfe, 2002, Lepvrier et al., 1997, Lepvrier et al., 2004 and Lepvrier et al., 2008). However, recent works argue that the SCB subducted beneath Indochina block along the Song Chay suture zone (Lepvrier et al., 2011 and Lin et al., 2011). Following Deprat (1915) and Lepvrier et al. (2011), a stack of nappes, and NE-verging recumbent folds characterize the structure of NE Vietnam.

In order to define precisely the time of this NE-verging synmetamorphic deformation, ^{40}Ar–^{39}Ar analyses were realized from gneiss and micaschist of the Song Chay massif. Biotite, muscovite and amphibole yield a large time span from 237 Ma to 115 Ma. These ages are interpreted as related to slow to moderate uplift in the Late Mesozoic, after the Triassic nappe stacking (Roger et al., 2000, Maluski et al., 2001 and Yan et al., 2006). From monazite inclusions in garnet, an age of 255–203 Ma was obtained by U–Th–Pb method (Gilley et al., 2003). All the available geochronological results obtained in the Song Chay massif are rather consistent but with a large time span. This led some geologists to consider the existence of a long thermal event during the early Mesozoic (Roger et al., 2000 and Carter et al., 2001). However, as the $^{40}Ar/^{39}Ar$ method is very sensitive to temperature, it does not appear a suitable method to discriminate the early tectonic and thermal events.

3. Sampling and analytical methods

3.1. Sample descriptions

All the six granitic samples come from the NE Vietnam (Fig. 2). Samples TK84 (N22°34.794′, E105° 52.709′, Fig. 2) and TK85 (N22°37.481′, E105°52.719′) are two mica leucogranites from the Pia Oac massif (Fig. 2), which is a small-scale undeformed pluton intruding the Devonian metasedimentary rocks. The granitic pluton is bounded by a normal fault and the surrounding rocks are mylonitic quartzite, micaschist and metapelite. Through microscopic observation (Fig. 4c and d), the major minerals of the samples are biotite (5–10%), muscovite (5–10%), quartz (25–30%), and feldspar (<50%). Sample TK216 (N21°50.690′, E105°00.209′, Fig. 2) is a biotite granite from the Bach Ha pluton (west of Tuyen Quang), which is an undeformed granitic pluton. The magmatic body is located north of the Song Chay suture zone and intrudes into foliated and lineated Devonian marble and paragneiss. Through microscopic observation (Fig. 4e), the major mineral components of the sample are biotite (10–15%), quartz (25–35%) and feldspar (<50%). Sample TK164 (N22°28.719′, E105°31.409′, Fig. 2) is a quartz-syenite from the Pia Ma massif (Fig. 2), which forms a crescent-shaped body convex to the east. This foliated and lineated pluton intrudes into the Devonian metapelites and marbles. Through microscopic observation (Fig. 4f), the major constitutive minerals of the sample are biotite (<5%), amphibole (15–20%), quartz (10–15%) and feldspar (<60%). Sample TK264 (N21°49.302′, E105°32.848′, Fig. 2) is a granodiorite from the large-scale Diem Mac granitic pluton (SW of Cho Chu, Fig. 2). This pluton, equivalent to the Phia Bioc massif (west of Bac Khan, Fig. 2), intrudes into foliated and weakly metamorphosed Ordovician pelitic rocks, and is covered by Upper Triassic conglomerates. Through the microscopic observation (Fig. 4g), the major mineral components of the sample are amphibole (20–30%), quartz (20–25%) and feldspar (<50%). Sample TK61 (N22°34.310′, E105°38.295′, Fig. 2) is a granodiorite from the Cổ Linh pluton (Fig. 2), which is a small-scale stock with a weak foliation, intruding into a ductilely deformed but unmetamorphosed Devonian pelite and thin bedded limestone series. Through microscopic observation (Fig. 4h), the major minerals are biotite (15–20%), quartz (10–15%), feldspar (<60%) and accessory minerals (<5%).

3.2. SIMS U–Pb dating methods

Zircon concentrates were separated from approximately 2 kg rock samples by conventional magnetic and density techniques to concentrate non-magnetic, heavy fractions. Zircon grains, together with 91,500, Plešovice, and Penglai zircon standards were mounted in epoxy mounts, which were then polished to section the crystals in half for analysis. All zircon structures were documented with transmitted and reflected light photomicrographs, as well as cathodoluminescence (CL) images, to reveal their internal structures. Each mount was vacuum-coated with high-purity gold prior to secondary ion mass spectrometry (SIMS) analysis.

Measurements of U, Th and Pb were conducted using the Cameca IMS-1280 SIMS at the Institute of Geology and Geophysics, Chinese Academy of Sciences at Beijing. U–Th–Pb ratios and absolute abundances were determined relative to the standard zircon Plešovice (Sláma et al., 2008) and 91,500 (Wiedenbeck et al., 1995), analyses of which were interspersed with those of unknown grains, using operating and data processing procedures similar to those described by Li et al. (2009). A long-term uncertainty of 1.5% (1 RSD) for $^{206}Pb/^{238}U$ measurements of the standard zircons was propagated to the unknowns (Li et al.,

2010b), despite that the measured $^{206}Pb/^{238}U$ error in a specific session is generally around 1% (1 RSD) or less. Measured compositions were corrected for common Pb using non-radiogenic ^{204}Pb. Corrections are sufficiently small to be insensitive to the choice of common Pb composition, and an average of present-day crustal composition (Stacey and Kramers, 1975) is used for the common Pb assuming that the common Pb is largely surface contamination introduced during sample preparation. Uncertainties on individual analyses in data tables are reported at a 1sigma level; mean ages for pooled U/Pb (and Pb/Pb) analyses are quoted with 95% confidence interval. Data reduction was carried out using the Isoplot/Ex v. 2.49 programs (Ludwig, 2001). SIMS zircon U–Pb isotopic data are presented in Table 2.

Table 2. : SIMS zircon U–Pb results.[a]

Sample	[U]	[Th]	[Pb]	Th	^{206}Pb	f_{206}	^{207}Pb	±1 σ	^{206}Pb	±1 σ	^{207}Pb	±1 σ	^{207}Pb	±1 σ	^{207}Pb	±1 σ	^{206}Pb	±1 σ
Spots	ppm	ppm	ppm	U	^{204}Pb	%	^{235}U	%	^{238}U	%	^{206}Pb	%	^{206}Pb		^{235}U		^{238}U	
TK61(22°34.310′,105°38.295′)																		
TK61@1	5818	4843	311	0.832	13946	{0.13}	0.29155	1.60	0.0410	1.50	0.05156	0.56	266.1	12.8	259.8	3.7	259.1	3.8
TK61@2	3001	1681	147	0.560	77791	{0.02}	0.28274	1.66	0.0402	1.50	0.05104	0.70	242.7	16.1	252.8	3.7	253.9	3.7
TK61@3	984	449	47	0.457	19316	{0.10}	0.28475	1.99	0.0398	1.50	0.05187	1.30	279.6	29.4	254.4	4.5	251.7	3.7
TK61@4	3182	2401	165	0.755	101677	{0.02}	0.28906	1.64	0.0406	1.50	0.05161	0.67	268.4	15.3	257.8	3.8	256.7	3.8
TK61@5	5442	3341	279	0.614	4372	{0.43}	0.29297	1.66	0.0415	1.50	0.05119	0.71	249.5	16.3	260.9	3.8	262.2	3.9
TK61@6	3816	2554	196	0.669	50216	{0.04}	0.28878	1.65	0.0410	1.50	0.05106	0.69	243.3	15.9	257.6	3.8	259.2	3.8
TK61@7	1823	779	85	0.427	71496	{0.03}	0.28158	1.75	0.0396	1.50	0.05151	0.90	263.5	20.6	251.9	3.9	250.7	3.7
TK61@8	2139	948	102	0.443	32746	{0.06}	0.27772	1.84	0.0402	1.50	0.05013	1.06	200.9	24.4	248.8	4.1	254.0	3.7
TK61@9	2834	1428	138	0.504	39776	{0.05}	0.28507	1.67	0.0405	1.50	0.05101	0.73	241.4	16.8	254.7	3.8	256.1	3.8
TK61@11*	2291	1011.02	100	0.441	95774.04	{0.20}	0.26467	1.78	0.0375	1.50	0.05120	0.96	250.0	21.8	238.4	3.8	237.2	3.5
TK61@10	1574	627	73	0.398	21546	{0.09}	0.28147	1.89	0.0398	1.51	0.05123	1.15	251.2	26.2	251.8	4.2	251.9	3.7
TK61@12	2918	1496	146	0.513	158261	{0.01}	0.29523	1.71	0.0413	1.50	0.05180	0.81	276.8	18.5	262.7	4.0	261.1	3.8
TK61@13*	8198	6803	451	0.830	1165	{1.61}	0.30159	2.39	0.0425	1.50	0.05142	1.86	259.6	42.1	267.6	5.6	268.6	3.9
TK61@14	5093	3359	264	0.660	113776	{0.02}	0.29241	1.59	0.0415	1.50	0.05105	0.53	243.2	12.2	260.5	3.7	262.4	3.9
TK61@15*	2582	34	255	0.013	228112	{0.01}	0.79884	1.68	0.0927	1.56	0.06250	0.63	691.2	13.4	596.2	7.6	571.5	8.5
TK61@16	3772	2445	192	0.648	81397	{0.02}	0.28890	1.63	0.0410	1.50	0.05111	0.63	245.7	14.5	257.7	3.7	259.0	3.8
TK61@17	773	87	34	0.113	19855	{0.09}	0.28226	2.15	0.0401	1.50	0.05104	1.54	242.7	35.2	252.5	4.8	253.5	3.7
TK61@18	2017	831	96	0.412	50505	{0.04}	0.28723	1.78	0.0406	1.50	0.05129	0.96	253.9	21.9	256.4	4.0	256.7	3.8

Sample	[U]	[Th]	[Pb]	Th	^{206}Pb	f_{206}	^{207}Pb	±1 σ	^{206}Pb	±1 σ	^{207}Pb	±1 σ	^{207}Pb	±1 σ	^{207}Pb	±1 σ	^{206}Pb	±1 σ
Spots	ppm	ppm	ppm	U	^{204}Pb	%	^{235}U	%	^{238}U	%	^{206}Pb	%	^{206}Pb		^{235}U		^{238}U	
TK61@19	2244	881	107	0.393	159317	{0.01}	0.29217	1.77	0.0408	1.50	0.05196	0.93	283.8	21.2	260.3	4.1	257.7	3.8
TK61@20	3935	2699	204	0.686	36341	{0.05}	0.29126	1.64	0.0411	1.50	0.05137	0.67	257.5	15.4	259.6	3.8	259.8	3.8
TK61@21	1441	238	63	0.165	10653	{0.18}	0.28141	1.95	0.0399	1.53	0.05109	1.21	245.1	27.6	251.8	4.4	252.5	3.8
TK61@22	3629	2323	187	0.640	140158	{0.01}	0.29515	1.63	0.0414	1.50	0.05176	0.63	274.8	14.3	262.6	3.8	261.2	3.8
TK61@23	5264	3198	271	0.608	7764	{0.24}	0.29521	1.63	0.0418	1.50	0.05126	0.64	252.6	14.7	262.6	3.8	263.8	3.9
TK84(22°34.794′,105°52.709′)																		
TK84@1	5692	804	93	0.141	3755	{0.50}	0.09933	2.14	0.0151	1.50	0.04779	1.52	89.1	35.6	96.2	2.0	96.4	1.4
TK84@2	936	1864	22	1.990	12963	{0.14}	0.09084	2.93	0.0141	1.50	0.04676	2.51	37.1	59.1	88.3	2.5	90.2	1.3
TK84@3	2606	243	40	0.093	23828	{0.08}	0.09332	2.21	0.0141	1.53	0.04812	1.60	105.3	37.3	90.6	1.9	90.0	1.4
TK84@4	1155	766	120	0.663	36152	{0.05}	0.64870	1.68	0.0829	1.50	0.05674	0.76	481.5	16.8	507.7	6.7	513.5	7.4
TK84@5	344	117	54	0.341	82349	{0.02}	1.23357	1.79	0.1331	1.50	0.06723	0.97	845.0	20.1	816.0	10.1	805.3	11.4
TK84@6	702	2327	20	3.314	6308	{0.30}	0.09167	4.78	0.0141	1.50	0.04722	4.54	60.5	104.8	89.1	4.1	90.1	1.3
TK84@7	1727	1235	32	0.715	35876	{0.05}	0.09740	2.31	0.0147	1.53	0.04810	1.74	104.0	40.5	94.4	2.1	94.0	1.4
TK84@8	1283	54	19	0.042	11392	{0.16}	0.09222	2.66	0.0141	1.51	0.04749	2.19	73.7	51.4	89.6	2.3	90.2	1.3
TK84@9	310	497	7	1.600	4415	{0.42}	0.09082	5.66	0.0142	1.59	0.04634	5.43	0.0	141.0	88.3	4.8	91.0	1.4
TK84@10	759	844	15	1.111	6119	{0.31}	0.09627	3.50	0.0146	1.52	0.04768	3.15	83.7	73.1	93.3	3.1	93.7	1.4
TK84@11	1989	1052	324	0.529	31420	{0.06}	1.21365	1.75	0.1318	1.68	0.06678	0.48	831.0	9.9	806.9	9.8	798.2	12.6
TK84@12	1194	320	19	0.268	8718	{0.21}	0.09209	2.46	0.0141	1.51	0.04753	1.94	76.1	45.6	89.4	2.1	89.9	1.4
TK84@13	446	97	70	0.218	108124	{0.02}	1.28638	1.74	0.1384	1.51	0.06740	0.85	850.2	17.6	839.7	10.0	835.7	11.9
TK84@14	1922	280	29	0.146	20656	{0.09}	0.09006	2.74	0.0139	1.52	0.04682	2.28	40.2	53.7	87.6	2.3	89.3	1.3
TK84@15	526	773	53	1.469	35006	{0.05}	0.51256	2.00	0.0670	1.54	0.05546	1.28	431.0	28.2	420.2	6.9	418.2	6.2
TK85(22°37.481′,105°52.719′)																		
TK85@1	531	319	9	0.601	9741	{0.19}	0.08935	4.89	0.0136	1.53	0.04770	4.64	84.4	106.6	86.9	4.1	87.0	1.3
TK85@2	488	354	9	0.725	9439	{0.20}	0.09446	4.17	0.0142	1.53	0.04827	3.88	112.5	89.2	91.7	3.7	90.8	1.4
TK85@3	41	71	64	0.1	3711	{0.0	1.26	1.	0.13	1.	0.06	1.	818.	22.	830.	10	835.	11

Sample	[U]	[Th]	[Pb]	Th	^{206}Pb	f_{206}	^{207}Pb	±1 σ	^{206}Pb	±1 σ	^{207}Pb	±1 σ	^{207}Pb	±1 σ	^{207}Pb	±1 σ	^{206}Pb	±1 σ
Spots	ppm	ppm	ppm	U	^{204}Pb	%	^{235}U	%	^{238}U	%	^{206}Pb	%	^{206}Pb		^{235}U		^{238}U	
	3			73	7	5}	608	86	83	51	639	09	5	6	6	.6	2	.8
TK85@4	4184	378	64	0.090	108208	{0.02}	0.09453	1.80	0.0142	1.51	0.04831	0.99	114.6	23.1	91.7	1.6	90.8	1.4
TK85@5	612	322	10	0.526	6762	{0.28}	0.08974	3.74	0.0138	1.54	0.04701	3.41	49.6	79.5	87.3	3.1	88.6	1.4
TK85@6	1992	493	32	0.248	38569	{0.05}	0.09468	2.10	0.0142	1.52	0.04832	1.44	115.0	33.7	91.9	1.8	91.0	1.4
TK85@7	513	695	11	1.356	5569	{0.34}	0.09533	3.23	0.0142	1.55	0.04878	2.83	137.1	65.2	92.5	2.9	90.7	1.4
TK85@8	3779	600	59	0.159	51949	{0.04}	0.09284	1.88	0.0143	1.50	0.04701	1.12	49.6	26.5	90.1	1.6	91.7	1.4
TK85@9	2898	5388	64	1.859	8201	{0.23}	0.09645	2.27	0.0144	1.51	0.04857	1.69	127.1	39.3	93.5	2.0	92.2	1.4
TK85@10	3823	380	59	0.099	51368	{0.04}	0.09517	1.87	0.0143	1.50	0.04841	1.11	119.5	26.0	92.3	1.7	91.3	1.4
TK85@11	1759	230	27	0.131	32908	{0.06}	0.09423	2.18	0.0143	1.52	0.04793	1.57	95.7	36.8	91.4	1.9	91.3	1.4
TK85@12	391	187	7	0.479	11307	{0.17}	0.09676	3.74	0.0139	1.79	0.05032	3.28	209.6	74.4	93.8	3.4	89.3	1.6
TK85@13	142	229	3	1.607		{0.00}	0.09049	6.60	0.0143	2.42	0.04583	6.14	−11.4	142.1	88.0	5.6	91.7	2.2
TK85@14	2311	535	38	0.231	25799	{0.07}	0.09725	2.23	0.0147	1.51	0.04789	1.64	93.7	38.4	94.2	2.0	94.3	1.4
TK85@15	896	661	16	0.737	9268	{0.20}	0.09037	3.17	0.0141	1.53	0.04660	2.77	28.8	65.1	87.9	2.7	90.0	1.4
TK85@16	1739	404	27	0.233	1625	{1.15}	0.08772	3.86	0.0140	1.52	0.04556	3.55	−25.8	83.9	85.4	3.2	89.4	1.4
TK85@17	2352	345	37	0.147	11101	{0.17}	0.09292	2.20	0.0145	1.51	0.04643	1.61	20.2	38.2	90.2	1.9	92.9	1.4
TK85@18	4124	471	63	0.114	226805	{0.01}	0.09468	1.84	0.0142	1.51	0.04839	1.05	118.4	24.6	91.9	1.6	90.8	1.4
TK85@19	338	814	9	2.410	10102	{0.19}	0.09198	4.08	0.0143	1.65	0.04652	3.73	24.5	87.0	89.3	3.5	91.8	1.5
TK85@20	394	824	9	2.091	2944	{0.64}	0.09717	3.64	0.0143	1.55	0.04934	3.30	164.0	75.3	94.2	3.3	91.4	1.4
TK164(22°28.719′,105°31.409′)																		
TK164@1	75	79	4	1.053	10535	{0.18}	0.29271	4.57	0.0386	1.55	0.05493	4.30	409.4	93.4	260.7	10.6	244.4	3.7
TK164@2	128	183	7	1.423	3972	{0.47}	0.27755	3.72	0.0391	1.62	0.05154	3.35	265.1	75.2	248.7	8.2	247.0	3.9
TK164@3	201	47	19	0.234	12068	{0.15}	0.69145	2.45	0.0851	1.50	0.05893	1.94	564.7	41.7	533.7	10.2	526.4	7.6
TK164@4	77	80	4	1.048		{0.00}	0.26272	5.53	0.0388	1.50	0.04908	5.32	151.5	120.1	236.9	11.7	245.5	3.6
TK164@5	324	514	19	1.589	4851	{0.39}	0.26347	3.83	0.0390	1.51	0.04898	3.52	146.9	80.5	237.5	8.1	246.7	3.7
TK164@6	445	344	49	0.773	38369	{0.05}	0.67671	1.92	0.0845	1.50	0.05810	1.20	533.7	26.1	524.8	7.9	522.7	7.5

Sample	[U]	[Th]	[Pb]	Th	^{206}Pb	f_{206}	^{207}Pb	±1 σ	^{206}Pb	±1 σ	^{207}Pb	±1 σ	^{207}Pb	±1 σ	^{207}Pb	±1 σ	^{206}Pb	±1 σ
Spots	ppm	ppm	ppm	U	^{204}Pb	%	^{235}U	%	^{238}U	%	^{206}Pb	%	^{206}Pb		^{235}U		^{238}U	
TK164@7	260	110	26	0.421	17647	{0.11}	0.66656	2.25	0.0839	1.53	0.05763	1.65	515.6	35.9	518.6	9.2	519.3	7.6
TK164@8	278	277	15	0.997		{0.00}	0.28322	2.74	0.0386	1.54	0.05316	2.26	335.8	50.4	253.2	6.1	244.4	3.7
TK164@9	233	134	24	0.574	70173	{0.03}	0.68767	2.23	0.0843	1.57	0.05915	1.59	572.5	34.1	531.4	9.3	521.9	7.9
TK164@10	175	141	9	0.804	6970	{0.27}	0.26069	3.35	0.0391	1.61	0.04833	2.94	115.3	67.9	235.2	7.1	247.4	3.9
TK164@11	105	34	11	0.326	7159	{0.26}	0.66343	3.31	0.0867	1.50	0.05548	2.95	431.6	64.4	516.7	13.5	536.2	7.7
TK164@12	181	178	10	0.982	3798	{0.49}	0.29522	4.92	0.0409	2.72	0.05233	4.10	299.9	90.9	262.7	11.4	258.5	6.9
TK164@13	79	75	4	0.956	4416	{0.42}	0.26054	4.91	0.0389	1.63	0.04856	4.63	126.8	105.6	235.1	10.4	246.1	3.9
TK164@14	365	614	22	1.684	14411	{0.13}	0.26529	2.78	0.0384	1.51	0.05014	2.33	201.3	53.3	238.9	5.9	242.8	3.6
TK164@15	618	144	27	0.234		{0.00}	0.27961	2.13	0.0389	1.51	0.05219	1.51	293.7	34.1	250.4	4.7	245.8	3.6
TK164@16	656	153	29	0.234	61018	{0.03}	0.27610	2.10	0.0389	1.50	0.05153	1.46	264.6	33.2	247.6	4.6	245.8	3.6
TK164@17	462	313	49	0.677	55832	{0.03}	0.67576	1.88	0.0843	1.50	0.05817	1.12	536.0	24.4	524.2	7.7	521.5	7.5
TK164@18	135	37	6	0.277	5416	{0.35}	0.27202	4.51	0.0383	1.53	0.05152	4.24	264.3	94.5	244.3	9.8	242.2	3.6
TK164@19	447	176	44	0.394	31419	{0.06}	0.66680	1.92	0.0848	1.50	0.05706	1.20	493.7	26.2	518.8	7.8	524.5	7.6
TK164@20	155	57	16	0.367	13869	{0.13}	0.69231	2.63	0.0861	1.50	0.05832	2.16	541.8	46.6	534.2	11.0	532.4	7.7
TK216(21°50.690′,105°00.209′)																		
TK216@1	1518	528	68	0.348	38112	{0.05}	0.26740	1.88	0.0387	1.50	0.05010	1.14	199.4	26.2	240.6	4.0	244.9	3.6
TK216@2	3054	1491	149	0.488	45660	{0.04}	0.28154	1.67	0.0404	1.50	0.05054	0.74	219.8	17.1	251.9	3.7	255.3	3.8
TK216@3*	1012	160	57	0.159	22098	{0.08}	0.36915	1.87	0.0494	1.51	0.05419	1.10	379.0	24.7	319.0	5.1	310.9	4.6
TK216@4	1146	369	51	0.322	18741	{0.10}	0.26463	1.97	0.0386	1.50	0.04977	1.27	184.3	29.3	238.4	4.2	243.9	3.6
TK216@5*	929	205	247	0.221	210169	{0.01}	2.85584	2.00	0.2299	1.77	0.09008	0.94	1427.3	17.9	1370.3	15.2	1334.1	21.3
TK216@6*	314	112	53	0.356	21930	{0.09}	1.38483	1.89	0.1429	1.51	0.07031	1.14	937.4	23.1	882.5	11.2	860.8	12.1
TK216@7*	3945	394	199	0.100	56443	{0.03}	0.33261	1.62	0.0462	1.51	0.05222	0.59	295.2	13.3	291.6	4.1	291.1	4.3
TK216@8	2993	615	134	0.205	45672	{0.04}	0.27957	1.67	0.0402	1.50	0.05041	0.72	213.8	16.6	250.3	3.7	254.2	3.7
TK216@9	2601	426	115	0.164	68516	{0.03}	0.28167	1.69	0.0400	1.50	0.05105	0.77	242.9	17.7	252.0	3.8	253.0	3.7
TK216@10	19	532	89	0.2	1799	{0.0	0.27	1.	0.03	1.	0.05	0.	254.	21.	250.	4.	249.	4.

Sample	[U]	[Th]	[Pb]	Th	^{206}Pb	f_{206}	^{207}Pb	±1 σ	^{206}Pb	±1 σ	^{207}Pb	±1 σ	^{207}Pb	±1 σ	^{207}Pb	±1 σ	^{206}Pb	±1 σ
Spots	ppm	ppm	ppm	U	^{204}Pb	%	^{235}U	%	^{238}U	%	^{206}Pb	%	^{206}Pb		^{235}U		^{238}U	
	83			68	04	1}	922	97	95	73	130	94	5	6	0	4	6	2
TK216@11*	1821	73	214	0.040	116051	{0.02}	1.01217	1.61	0.1096	1.54	0.06695	0.49	836.3	10.1	710.0	8.3	670.7	9.8
TK216@12	2655	294	117	0.111	37248	{0.05}	0.28025	1.69	0.0406	1.50	0.05011	0.77	199.9	17.8	250.9	3.8	256.3	3.8
TK216@13	2347	609	104	0.259	4177	{0.45}	0.27893	1.89	0.0394	1.50	0.05140	1.15	259.0	26.2	249.8	4.2	248.8	3.7
TK216@14*	3063	402	143	0.131	154538	{0.01}	0.30767	1.64	0.0428	1.50	0.05208	0.65	288.9	14.8	272.4	3.9	270.5	4.0
TK216@15	4346	458	195	0.105	69010	{0.03}	0.29260	1.61	0.0415	1.50	0.05118	0.59	248.9	13.4	260.6	3.7	261.9	3.9
TK216@16	2376	380	105	0.160	37143	{0.05}	0.27863	1.73	0.0403	1.50	0.05014	0.86	201.5	19.9	249.6	3.8	254.7	3.7
TK216@17	2283	960	107	0.421	39294	{0.05}	0.28023	1.71	0.0399	1.50	0.05097	0.83	239.6	19.0	250.8	3.8	252.0	3.7
TK216@18	3477	589	157	0.169	90255	{0.02}	0.28676	1.64	0.0410	1.50	0.05078	0.66	230.7	15.1	256.0	3.7	258.8	3.8
TK216@19	1677	401	76	0.239	46137	{0.04}	0.28195	1.85	0.0402	1.50	0.05092	1.08	237.1	24.8	252.2	4.1	253.8	3.7
TK216@20	2821	1211	135	0.429	43533	{0.04}	0.28205	1.82	0.0405	1.50	0.05050	1.03	218.0	23.7	252.3	4.1	256.0	3.8
TK216@21	4125	2158	201	0.523	33858	{0.06}	0.28074	1.67	0.0401	1.51	0.05076	0.72	229.9	16.5	251.2	3.7	253.5	3.8
TK264(21°49.302′,105°32.848′)																		
TK264@1*	490	152	76	0.310	62515	{0.03}	1.48097	1.84	0.1276	1.68	0.08415	0.76	1296.1	14.8	922.6	11.2	774.4	12.3
TK264@2	753	165	34	0.219		{0.00}	0.29114	2.48	0.0402	1.50	0.05253	1.98	308.5	44.4	259.5	5.7	254.1	3.7
TK264@3	591	252	27	0.426	31911	{0.06}	0.27603	2.15	0.0391	1.50	0.05123	1.54	251.2	35.1	247.5	4.7	247.1	3.6
TK264@4	514	215	24	0.417	19973	{0.09}	0.27671	2.26	0.0398	1.52	0.05048	1.67	217.2	38.2	248.0	5.0	251.3	3.7
TK264@5	751	158	33	0.211	19415	{0.10}	0.27877	2.03	0.0398	1.50	0.05080	1.37	231.7	31.4	249.7	4.5	251.6	3.7
TK264@6	597	325	29	0.544	52201	{0.04}	0.28279	2.41	0.0395	1.51	0.05192	1.88	281.7	42.4	252.9	5.4	249.8	3.7
TK264@7*	827	292	39	0.354	1809	{1.03}	0.28466	9.32	0.0404	1.50	0.05106	9.20	243.7	199.1	254.3	21.2	255.5	3.8
TK264@8*	594	378	117	0.637	91458	{0.02}	1.60039	1.66	0.1552	1.50	0.07478	0.70	1062.7	14.0	970.4	10.4	930.1	13.0
TK264@9*	435	179	20	0.410	1228	{1.52}	0.27704	7.22	0.0389	1.52	0.05169	7.05	271.8	154.1	248.3	16.0	245.8	3.7
TK264@10	416	153	19	0.367		{0.00}	0.28697	2.71	0.0401	1.51	0.05196	2.25	283.8	50.7	256.2	6.2	253.2	3.7
TK264@11*	1239	262	57	0.212		{0.00}	0.28908	1.83	0.0409	1.50	0.05127	1.05	253.0	23.9	257.8	4.2	258.4	3.8
TK264@12	396	174	19	0.440	12490	{0.15}	0.28154	2.48	0.0399	1.51	0.05123	1.97	251.1	44.6	251.9	5.5	252.0	3.7

Sample	[U]	[Th]	[Pb]	Th	^{206}Pb	f_{206}	^{207}Pb	±1 σ	^{206}Pb	±1 σ	^{207}Pb	±1 σ	^{207}Pb	±1 σ	^{207}Pb	±1 σ	^{206}Pb	±1 σ
Spots	ppm	ppm	ppm	U	^{204}Pb	%	^{235}U	%	^{238}U	%	^{206}Pb	%	^{206}Pb		^{235}U		^{238}U	
TK264@13	1237	248	55	0.200	72360	{0.03}	0.28749	1.84	0.0401	1.50	0.05202	1.05	286.1	23.9	256.6	4.2	253.4	3.7
TK264@14	717	142	32	0.198	23168	{0.08}	0.28113	2.47	0.0403	1.50	0.05055	1.96	220.3	44.7	251.6	5.5	254.9	3.8
TK264@15	1039	148	46	0.142	17734	{0.11}	0.28819	2.32	0.0404	1.50	0.05169	1.77	271.6	40.1	257.1	5.3	255.6	3.8
TK264@16	1247	379	57	0.304	67253	{0.03}	0.29063	1.84	0.0400	1.50	0.05266	1.06	314.0	23.9	259.1	4.2	253.0	3.7
TK264@17	454	172	21	0.379	9931	{0.19}	0.27462	2.51	0.0396	1.50	0.05028	2.01	207.8	46.1	246.4	5.5	250.4	3.7
TK264@18*	1779	742	86	0.417	47343	{0.04}	0.28913	1.78	0.0412	1.50	0.05089	0.96	235.9	22.0	257.9	4.1	260.3	3.8
TK264@19	601	276	28	0.459	100737	{0.02}	0.27488	2.15	0.0393	1.51	0.05069	1.53	226.7	34.9	246.6	4.7	248.7	3.7
TK264@20	551	301	26	0.546	12351	{0.15}	0.27453	2.75	0.0393	1.51	0.05066	2.31	225.4	52.4	246.3	6.0	248.5	3.7
TK264@21	565	205	26	0.363		{0.00}	0.28198	2.15	0.0394	1.50	0.05193	1.54	282.4	34.8	252.2	4.8	249.0	3.7
TK264@22	1358	590	65	0.434	44271	{0.04}	0.28678	1.97	0.0405	1.51	0.05138	1.26	25					

3.3. SIMS zircon oxygen isotope measurement

Samples for zircon oxygen isotopes were measured using the Cameca IMS-1280 SIMS at the Institute of Geology and Geophysics in the Chinese Academy of Sciences, Beijing. The original mounts were re-ground and polished to remove any trace of the analytical pits after U–Pb dating. The Cs+ primary ion beam was accelerated at 10 kV, with an intensity of ca.2 nA (Gaussian mode with a primary beam aperture of 200 μm to reduce aberrations) and rastered over a 10 μm area. The spot size is about 20 μm in diameter. The normal incidence electron flood gun was used to compensate for sample charging during analysis with homogeneous electron density over a 100 μm oval area. 60 ev energy window was used, together with a mass resolution of ca.2500. Oxygen isotopes were measured using multi-collection mode on two off-axis Faraday cups. The intensity of ^{16}O was typically 1 × 109 cps. The NMR (Nuclear Magnetic Resonance) probe was used for magnetic field control with stability better than 3 ppm over 16 h on mass 17. One analysis takes ca. 5 min consisting of pre-sputtering (~120 s), automatic beam centering (~60 s) and integration of oxygen isotopes (20 cycles × 4 s, total 80 s). Uncertainties on individual analyses are usually better than 0.2–0.3‰ (1σ).

The instrumental mass fractionation (IMF) factor is corrected using zircon 91,500 standard with a δ^{18}O value of 9.9 ± 0.3‰ (Wiedenbeck et al., 2004) and Penglai zircon standard (δ^{18}O VSMOW = 5.3‰) (Li et al., 2010). The internal precision of a single analysis generally was better than 0.2‰ (1σ standard error) for the ^{18}O/^{16}O ratio. Measured ^{18}O/^{16}O ratios were normalized by using Vienna Standard Mean Ocean Water compositions (VSMOW, ^{18}O/^{16}O = 0.0020052), and then corrected for the instrumental mass fractionation factor (IMF) as follows:

$$(\delta^{18}\mathrm{O})\mathrm{M}\left[\frac{(^{18}\mathrm{O}/^{16}\mathrm{O})\mathrm{M}}{0.0020052}-1\right]\times 1000(‰).$$

IMF=$(\delta^{18}O)_{M(standard)}$-$(\delta^{18}O)_{VSMOW}$,

$\delta^{18}O_{sample}=(\delta^{18}O)_{M}$+IMF

Zircon oxygen isotopic data are listed in Table 3.

Table 3. : In situ zircon Hf–O isotopic results.

Spot[a]	$^{176}Lu/^{177}Hf$	$^{176}Hf/^{177}Hf$	±2 σ_m	$\varepsilon_{Hf}(t)$	T_{DM}^{C} (Ma)	$\delta^{18}O$ (‰)	±2 σ_m
Coˇ Linh pluton (Granodiorite TK61, 254.8 Ma)							
TK61@1	0.001737	0.282497	0.000018	−4.3	1563	9.20	0.32
TK61@2	0.001106	0.282498	0.000017	−4.3	1558	9.26	0.38
TK61@3	0.000866	0.282500	0.000017	−4.2	1552	9.61	0.24
TK61@4	0.001853	0.282515	0.000018	−3.8	1527	9.54	0.20
TK61@5	0.001476	0.282486	0.000015	−4.6	1583	8.46	0.18
TK61@6	0.001427	0.282532	0.000017	−3.0	1482	9.62	0.27
TK61@7	0.003722	0.282527	0.000021	−3.8	1521	8.79	0.36
TK61@8	0.001917	0.282513	0.000019	−3.9	1532	9.95	0.37
TK61@9	0.001289	0.282544	0.000014	−2.7	1456	9.29	0.32
TK61@10	0.001794	0.282501	0.000019	−4.7	1567	9.86	0.24
TK61@12	0.001335	0.282514	0.000017	−3.6	1520	9.43	0.34
TK61@14	0.001739	0.282513	0.000018	−3.7	1527	9.47	0.26
TK61@16	0.001805	0.282475	0.000019	−5.1	1614	9.51	0.31
TK61@17	0.002172	0.282566	0.000019	−2.1	1417	9.15	0.37
TK61@18	0.001561	0.282473	0.000020	−5.2	1618	9.47	0.39
TK61@19	0.000972	0.282511	0.000018	−3.7	1525	9.12	0.25
TK61@20	0.001520	0.282526	0.000020	−3.3	1497	9.65	0.28
TK61@21	0.001473	0.282512	0.000020	−3.9	1531	9.59	0.20
TK61@22	0.001417	0.282531	0.000020	−3.0	1483	8.86	0.28
TK61@23	0.001449	0.282512	0.000017	−3.7	1524	9.05	0.27
Nà Giao pluton (Granites TK84,TK85, 90 Ma)							
TK84@2	0.001459	0.282534	0.000016	−6.5	1570	8.19	0.34
TK84@3	0.001112	0.282467	0.000011	−8.9	1719	9.87	0.16
TK84@6	0.002208	0.282643	0.000015	−2.7	1330	8.69	0.30
TK84@8	0.001121	0.282529	0.000013	−6.7	1580	9.52	0.30
TK84@9	0.001013	0.282580	0.000014	−4.9	1466	8.17	0.25
TK84@12	0.000717	0.282424	0.000016	−10.4	1812	9.17	0.22

Spot[a]	$^{176}Lu/^{177}Hf$	$^{176}Hf/^{177}Hf$	±2 σ_m	ε_{Hf} (*t*)	T_{DM}^{C} (Ma)	$\delta^{18}O$ (‰)	±2 σ_m
TK84@14	0.001407	0.282456	0.000013	−9.3	1744	9.38	0.23
TK85@4	0.001326	0.282494	0.000016	−7.8	1654	9.95	0.30
TK85@6	0.000778	0.282508	0.000012	−7.4	1625	10.95	0.37
TK85@9	0.002766	0.282564	0.000022	−5.5	1508	9.54	0.22
TK85@10	0.001259	0.282464	0.000015	−9.0	1724	9.78	0.21
TK85@11	0.000841	0.282383	0.000015	−11.8	1903	8.12	0.24
TK85@12	0.000257	0.282478	0.000016	−8.5	1692	9.34	0.23
TK85@13	0.000667	0.282552	0.000017	−5.8	1526	9.39	0.26
TK85@17	0.000150	0.282481	0.000016	−8.4	1687	9.55	0.25
TK85@18	0.000336	0.282463	0.000015	−9.0	1727	9.89	0.35
TK85@20	0.000438	0.282536	0.000017	−6.4	1565	8.24	0.29
TK85@21	0.000115	0.282529	0.000014	−6.7	1579	8.28	0.23
TK85@24	0.000695	0.282532	0.000013	−6.6	1574	8.54	0.26
TK85@25	0.000274	0.282449	0.000016	−9.5	1758	9.92	0.34
TK85@26	0.000058	0.282530	0.000023	−6.6	1578	9.71	0.23
TK85@28	0.001598	0.282521	0.000015	−7.0	1600	8.42	0.44
TK85@29	0.000006	0.282463	0.000013	−9.0	1724	9.62	0.31
Hong Thái pluton (Quartz−syenite TK164, 245 Ma)							
TK164@1	0.000718	0.282619	0.000027	−0.2	1289	4.61	0.29
TK164@2	0.000646	0.282574	0.000028	−1.7	1387	4.14	0.31
TK164@4	0.000894	0.282558	0.000023	−2.3	1426	4.04	0.30
TK164@5	0.001974	0.282567	0.000027	−2.2	1417	3.99	0.30
TK164@8	0.001609	0.282566	0.000025	−2.2	1417	4.74	0.35
TK164@10	0.000588	0.282563	0.000022	−2.1	1411	4.09	0.30
TK164@12	0.000867	0.282460	0.000026	−5.5	1637	4.32	0.35
TK164@13	0.001159	0.282576	0.000032	−1.7	1389	4.06	0.39
TK164@14	0.001920	0.282529	0.000027	−3.6	1503	4.14	0.21
TK164@15	0.001020	0.282554	0.000026	−2.5	1437	3.99	0.24
TK164@16	0.000393	0.282428	0.000026	−6.8	1712	4.33	0.45
TK164@18	0.000771	0.282541	0.000023	−3.0	1465	4.39	0.33
Hong Thái pluton (Quartz-syenite TK164, 525 Ma)							
TK164@3	0.000922	0.282497	0.000019	1.5	1399	4.63	0.35
TK164@6	0.001249	0.282524	0.000029	2.3	1347	5.26	0.16
TK164@7	0.001208	0.282512	0.000031	1.8	1377	4.62	0.19
TK164@9	0.000631	0.282476	0.000026	0.8	1443	4.32	0.26
TK164@11	0.000725	0.282452	0.000028	0.2	1490	4.64	0.33
TK164@17	0.001029	0.282546	0.000029	3.1	1294	5.13	0.29
TK164@19	0.001223	0.282492	0.000028	1.2	1418	4.38	0.30
TK164@20	0.000648	0.282527	0.000027	2.8	1323	4.56	0.32
Bach Ha pluton (Biotite granite TK216, 227.7 Ma)							

Spot[a]	$^{176}Lu/^{177}Hf$	$^{176}Hf/^{177}Hf$	±2 σ_m	ε_{Hf} (*t*)	T_{DM}^{C} (Ma)	$\delta^{18}O$ (‰)	±2 σ_m
TK216@1	0.001427	0.282362	0.000016	−9.4	1869	9.62	0.23
TK216@2	0.001957	0.282423	0.000016	−7.1	1734	9.79	0.30
TK216@4	0.001724	0.282397	0.000016	−8.2	1795	10.23	0.28
TK216@8	0.001841	0.282425	0.000019	−7.0	1728	9.42	0.31
TK216@9	0.001805	0.282453	0.000019	−6.0	1666	9.68	0.42
TK216@10	0.002722	0.282423	0.000020	−7.3	1745	9.46	0.27
TK216@12	0.002359	0.282423	0.000018	−7.1	1737	9.70	0.27
TK216@13	0.002487	0.282448	0.000020	−6.4	1688	9.37	0.28
TK216@16	0.002749	0.282409	0.000022	−7.7	1774	8.94	0.28
TK216@17	0.001735	0.282394	0.000021	−8.1	1798	9.08	0.41
TK216@18	0.002514	0.282420	0.000020	−7.2	1745	9.65	0.32
TK216@19	0.002794	0.282426	0.000016	−7.1	1736	9.32	0.39
TK216@20	0.001820	0.282399	0.000021	−7.9	1784	9.55	0.31
Drem Mac pluton (Granodiorite TK264, 251.8 Ma)							
TK264@2	0.000953	0.282375	0.000013	−8.6	1829	11.08	0.25
TK264@3	0.000701	0.282354	0.000014	−9.5	1879	10.74	0.23
TK264@4	0.000875	0.282337	0.000014	−10.0	1915	11.15	0.34
TK264@5	0.000978	0.282389	0.000013	−8.2	1800	11.59	0.30
TK264@6	0.000704	0.282381	0.000012	−8.5	1816	11.41	0.19
TK264@7	0.001064	0.282421	0.000013	−7.0	1728	12.69	0.27
TK264@9	0.001247	0.282408	0.000014	−7.7	1766	11.47	0.40
TK264@10	0.000628	0.282390	0.000012	−8.1	1795	12.07	0.32
TK264@11	0.001243	0.282413	0.000012	−7.2	1746	10.83	0.24
TK264@12	0.000824	0.282379	0.000013	−8.5	1822	11.25	0.21
TK264@13	0.001300	0.282380	0.000014	−8.5	1822	12.17	0.25
TK264@14	0.001080	0.282393	0.000013	−8.0	1791	11.31	0.30
TK264@15	0.000914	0.282415	0.000015	−7.2	1741	10.61	0.28
TK264@16	0.001266	0.282411	0.000012	−7.4	1755	10.88	0.29
TK264@17	0.000919	0.282371	0.000012	−8.8	1841	10.74	0.20
TK264@18	0.001517	0.282357	0.000014	−9.2	1873	10.71	0.20
TK264@19	0.001079	0.282395	0.000010	−8.1	1790	11.53	0.26
TK264@20	0.001021	0.282342	0.000012	−9.9	1908	11.13	0.31
TK264@21	0.001026	0.282402	0.000013	−7.8	1773	11.49	0.32
TK264@22	0.000930	0.282458	0.000013	−5.6	1644	12.81	0.35

The spots with asterisk do not calculate as concordia age.

a

The analysis were conducted in the same spot as the SIMS U–Pb spot.
$\varepsilon_{Hf}(T) = [^{176}Hf/^{177}Hf_Z/^{176}Hf/^{177}Hf_{CHUR(T)}-1] \times 10{,}000$;

$^{176}Hf/^{177}Hf_{CHUR(T)} = {}^{176}Hf/^{177}Hf_{CHUR(0)} - {}^{176}Lu/^{177}Hf_{CHUR} \times (e^{\lambda T} - 1)$;
$T_{DM} = (1/\lambda) \times \ln[1 + (^{176}Hf/^{177}Hf_{DM} - {}^{176}Hf/^{177}Hf_Z)/(^{176}Lu/^{177}Hf_{DM} - {}^{176}Lu/^{177}Hf_Z)]$;
$T_{DM}^C = T_{DM} - (T_{DM} - T) \times [(f_{CC} - f_Z)/(f_{CC} - f_{DM})]$; $f_{Lu/Hf} = {}^{176}Hf/^{177}Hf_Z/^{176}Lu/^{177}Hf_{CHUR} - 1$, where f_{CC}, f_Z and f_{DM} are the $f_{Lu/Hf}$ values of the continental crust, zircon sample and the depleted mantle; subscript Z = analyzed zircon sample, CHUR = chondritic uniform reservoir; DM = depleted mantle; T is timing of the granitoids crystallization; $\lambda = 1.867 \times 10{-}11$ year−1, decay constant of ^{176}Lu (Söderlund et al., 2004); $^{176}Hf/^{177}Hf_{DM} = 0.28325$; $^{176}Lu/^{177}Hf_{DM} = 0.0384$; present-day $^{176}Hf/^{177}Hf_{CHUR(0)} = 0.282772$; $^{176}Hf/^{177}Hf_{CHUR} = 0.0332$; $^{176}Hf/^{177}Hf_{CC} = 0.015$. T_{DM} represents the model age calculated from the measured $^{176}Hf/^{177}Hf$ and $^{176}Lu/^{177}Hf$ ratios of a zircon, giving a minimum limit for the crustal residence age of the hafnium in the zircon; whereas T_{DM}^C , a "crust Hf model age," is derived from projecting the initial $^{176}Hf/^{177}Hf$ of a zircon with a Lu/Hf ratio corresponding to the continental crust back to the depleted mantle model growth curve. Thus, T_{DM}^C can represent the mean crustal residence age of the source material extracted from the depleted mantle.

3.4. LA-MC-ICPMS zircon Lu–Hf isotope measurements

In situ zircon Lu-Hf isotopic analysis was carried out on a Neptune multi-collector ICPMS equipped with a Geolas-193 laser-ablation system (LA-MC-ICPMS) at the Institute of Geology and Geophysics, Beijing. Lu-Hf isotopic measurements were made on the same zircon grains previously analyzed for U–Pb and O isotopes, with ablation pit of 63 μm in diameter, repetition rate of 8–10 Hz, laser beam energy density of 10 J/cm^2, and ablation time of 26 s. The detailed analytical procedures were similar to those described by Wu et al. (2006). Contribution of isobaric interferences by ^{176}Lu and ^{176}Yb on the ^{176}Hf signal were subtracted by monitoring the intensity of ^{175}Lu and ^{172}Yb signals, using $^{176}Lu/^{175}Lu = 0.026549$ and $^{176}Yb/^{172}Yb = 0.5886$ (Chu et al., 2002). Independent mass bias factors for Hf and Yb (β_{Hf} and β_{Yb}) in the isobaric interference correction were used. Measured $^{176}Hf/^{177}Hf$ ratios were normalized to $^{179}Hf/^{177}Hf = 0.7325$. Further external adjustment is not applied for the unknowns because our determined $^{176}Hf/^{177}Hf$ ratios of 0.282303 ± 0.000020 for zircon standards 91,500 are in good agreement with the reported values (Wu et al., 2006a). All the Lu-Hf isotope analysis results are listed in Table 3 with the error in 2σ of the mean.

3.5. Bulk-rock Sr–Nd isotopic analysis

Sr and Nd isotopic compositions were measured on a Finnigan Mat 262 thermal ionization mass spectrometer at the Institute of Geology and Geophysics in the Chinese Academy of Sciences, Beijing, following the procedure described in Zhang et al. (2008). Procedural blanks were < 100 pg for Sm and Nd and <500 pg for Rb and Sr. $^{143}Nd/^{144}Nd$ was corrected for mass fractionation by normalization to $^{146}Nd/^{144}Nd = 0.7219$, and $^{87}Sr/^{86}Sr$ ratios were normalized to $^{86}Sr/^{88}Sr = 0.1194$. The measured values for the NBS-987 Sr standard were $^{87}Sr/^{86}Sr = 0.710228 \pm 0.000010$ (2σ_m) during the period of data acquisition. Bulk-rock Sr–Nd isotopic data are listed in Table 4

Table 4. : Bulk-rock Sr–Nd isotopic results.

Sample No.	Rb (ppm)	Sr (ppm)	Sm (ppm)	Nd (ppm)	$^{147}Sm/^{144}Nd$	$^{87}Rb/^{86}Sr$	$^{143}Nd/^{144}Nd$	Error (±2 σ_m)	$^{87}Sr/^{86}Sr$	Error (±2 σ_m)	$(^{87}Sr/^{86}Sr)i$	Initial Nd	$\varepsilon_{Nd}(t)$
TK6	172	309	5.8	37.	0.0947	1.61	0.5119	0.000	0.716	0.000	0.7105	0.511	−9.

Sample No.	Rb (ppm)	Sr (ppm)	Sm (ppm)	Nd (ppm)	$^{147}Sm/^{144}Nd$	$^{87}Rb/^{86}Sr$	$^{143}Nd/^{144}Nd$	Error (±2 σ_m)	$^{87}Sr/^{86}Sr$	Error (±2 σ_m)	$(^{87}Sr/^{86}Sr)i$	Initial Nd	$\varepsilon_{Nd}(t)$
1	.3	.9	8	6			59	014	363	011		802	7
TK84	665.9	39.0	3.35	15.2	0.1333	49.5	0.512034	0.000015	0.788359	0.000013	0.7251	0.511956	−11.0
TK85	648.5	39.9	3.67	16.2	0.1370	47.0	0.512061	0.000015	0.788476	0.000011	0.728		

Notes: $I_{Sr} = (^{87}Sr/^{86}Sr)_{sample} - (^{87}Rb/^{86}Sr)_{sample} \times (e^{\lambda t} - 1)$, $\lambda = 1.42 \times 10{-}11$ year−1 (Steiger and Jäger, 1977); initial Nd = $(^{143}Nd/^{144}Nd)_{sample} - (^{147}Sm/^{144}Nd)_{sample} \times (e^{\lambda t} - 1)$,
$\varepsilon_{Nd} = ((^{143}Nd/^{144}Nd)_{sample}/(^{143}Nd/^{144}Nd)_{CHUR} - 1) \times 10000$,
$f_{Sm/Nd} = (^{147}Sm/^{144}Sm)_{sample}/(^{147}Sm/^{144}Sm)_{CHUR} - 1$,
$T_{DM1} = 1/\lambda \times \ln(1 + ((^{143}Nd/^{144}Nd)_{sample} - 0.51315)/((^{147}Sm/^{144}Nd)_{sample} - 0.2137)$, where $(^{147}Sm/^{144}Nd)_{CHUR} = 0.1967$, $(^{143}Nd/^{144}Nd)_{CHUR} = 0.512638$, $\lambda_{Sm} = 6.54 \times 10{-}12$ year^{-1} (Lugmair and Marti, 1978); $T_{DM2} = T_{DM1} - (T_{DM1} - t) \times (f_{cc} - f_{sample})/(f_{cc} - f_{DM})$, where $f_{cc} = -0.4$, $f_{DM} = 0.0859$.

.

4. Analytical results

4.1. Zircon U–Pb geochronology

Zircon grains selected from these six samples (TK61, TK84, TK85, TK164, TK216, TK264) are mostly euhedral to subhedral, transparent and colorless, ranging from 50 μm to 210 μm in length, and have length to width ratio between 1:1 to 3:1. Cathodoluminescence images show that representative zircons have commonly concentric oscillatory zoning with low to variable luminescence that indicates a magmatic origin (Fig. 5). The Th/U ratios of all samples are between 0.04 and 3.3, almost all Th/U ratios are ranging from 0.1 to 1.0, except a few zircons with low Th/U ratios. U–Pb data sets for all samples are given in Table 2.

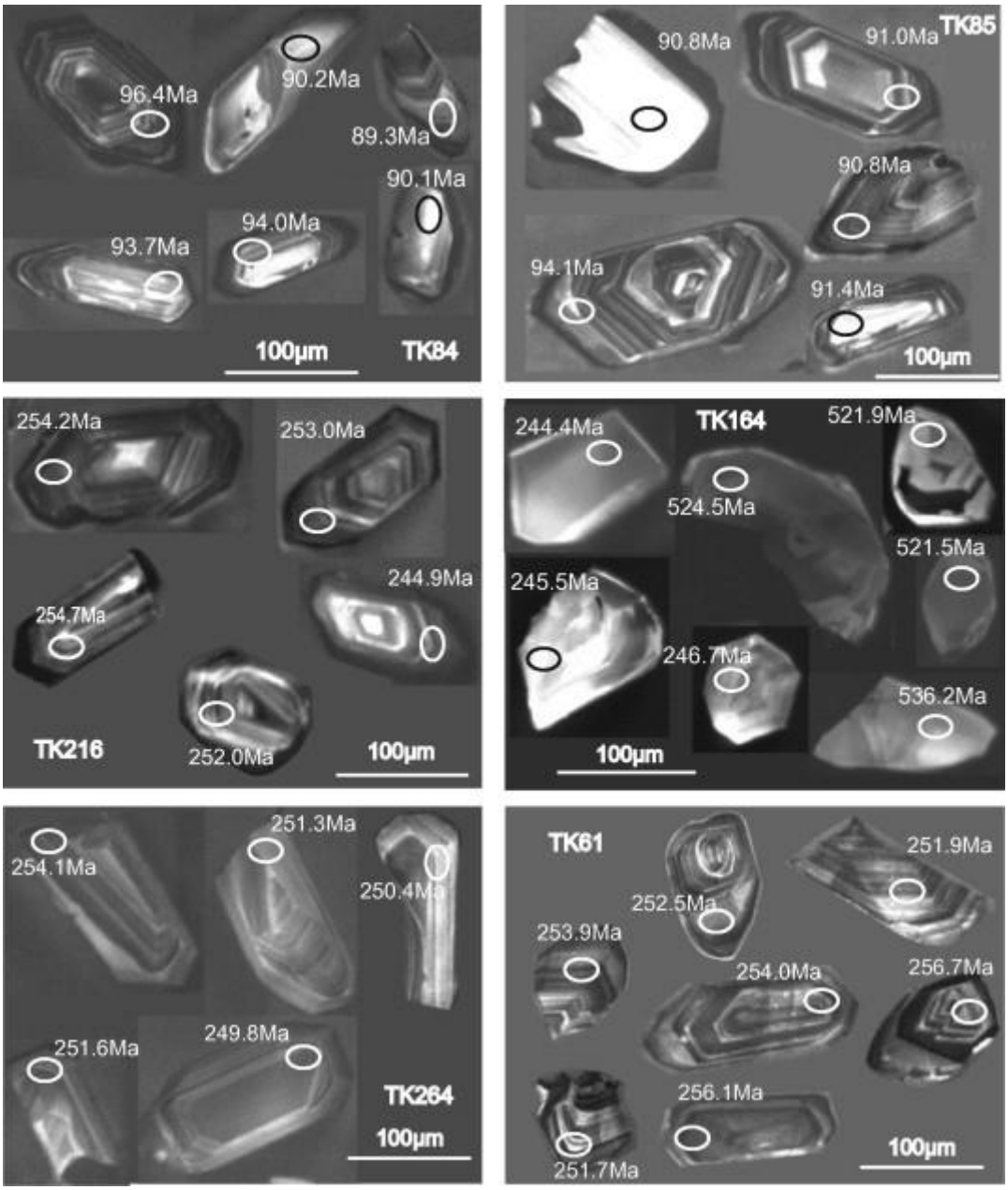

Fig. 5. : Cathodoluminescence images of representative zircons analyzed in situ for U–Pb, Hf and O isotopes. Small ellipses indicate the SIMS analysis spots for U–Pb isotopes. Numbers near the analysis spots are the U–Pb ages.

4.1.1. Two-mica Leucogranites (TK84, TK85)

Zircon grains in these samples are euhedral to subhedral, ranging from 50 μm to 200 μm in length, with length to width ratios between 1:1 and 3:1. Euhedral concentric zoning is common, and some grains have inherited cores (Fig. 5). Fifteen grains of sample TK84 were analyzed by SIMS, these analyses have variable concentrations of uranium (310–5692 ppm) and thorium (54–2327 ppm), with Th/U ratios ranging from 0.042 to 3.314, two Th/U ratios are less than 0.1. Three analyses give relatively older ages of 831 Ma, 845 Ma and 852 Ma, two analyzes yield ages of 513 Ma and 418 Ma, these may be due to inherited grains, and three nearly concordant ages of ca.94 Ma. Seven analyses yield a concordia age of

90.1 ± 1.0 Ma, which is interpreted as the crystallization age of the two mica leucogranite (Fig. 6a).

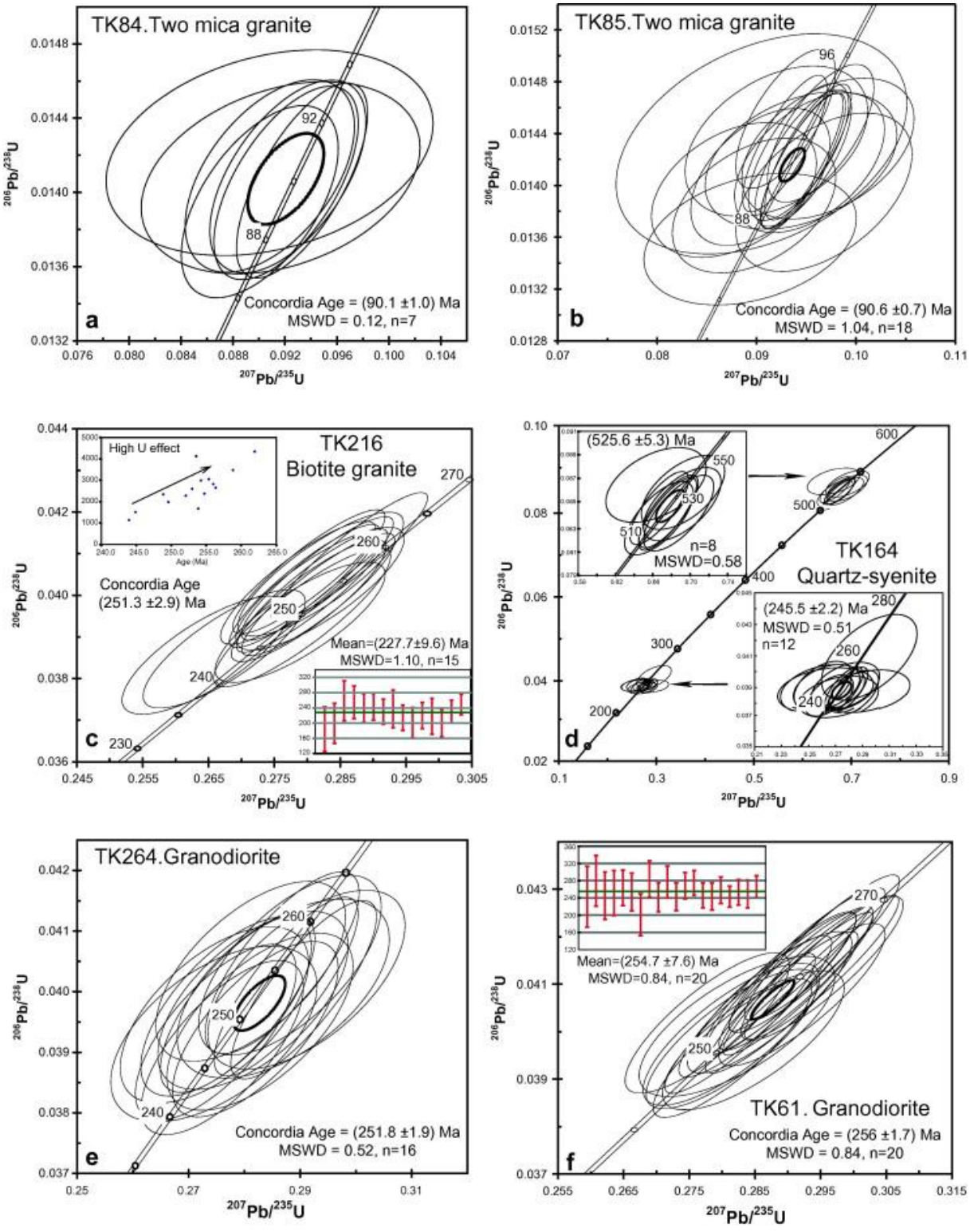

Fig. 6. : Conventional SIMS U–Pb zircon concordia diagram for the dated samples of northern Vietnam granitic rocks.

Twenty grains of sample TK85 were analyzed by SIMS, uranium and thorium concentrations are as follows: U = 142–4184 ppm and Th = 187–5318 ppm, with Th/U ratios ranging from 0.09 to 2.41, two Th/U ratios are less than 0.1. One grain gives a relatively old age at 818 Ma, while another one gives a nearly concordant age at 94.3 Ma. Eighteen analyses yield a concordia age of 90.6 ± 0.7 Ma (Fig. 6b). This age is consistent with the age of sample TK84 and is interpreted as the crystallization age of the two mica leucogranite.

4.1.2. Biotite granite (TK216)

Zircon grains in the TK216 sample are dominantly euhedral, ranging from 50 μm to 150 μm in length, with length to width ratios between 1:1 and 2:1. Concentric zoning is common, and some grains have inherited zircon cores (Fig. 5). Twenty-one grains were analyzed by SIMS, uranium and thorium concentrations are as follows: U = 1146–4346 ppm and a major population of Th = 294–2158 ppm, with Th/U ratios ranging from 0.105 to 0.523. Six analyses give relatively old ages and may be from the inherited zircons. Fifteen analyses yield a concordia age of 251.3 ± 2.9 Ma (Fig. 6c). But, these analyses show "high uranium effect", the ages become older while the uranium concentrations go higher (Li et al., 2010a, Fig. 6e). Thus, the realistic age maybe younger than this analyzed age. Considering that the $^{207}Pb/^{206}Pb$ ages are not affected by the high uranium concentration, the weighted mean $^{207}Pb/^{206}Pb$ age of 227.7 ± 9.6 Ma (MSWD = 1.1) (Fig. 6c) can be considered as the emplacement age of the pluton.

4.1.3. Quartz-syenite (TK164)

Zircon grains from this sample are subhedral, ranging from 50 μm to 150 μm in length, with length to width ratios between 1:1 and 1.5:1. Concentric oscillatory zoning is not clear, and most of the grains have inherited zircon cores (Fig. 5). Twenty analyses yield two groups of concordia age (Fig. 6d). One group is at 245.5 ± 2.2 Ma; these analyses have variable concentrations of uranium (75–656 ppm) and thorium (37–614 ppm), with Th/U ratios ranging from 0.234 to 1.684, which indicates a magmatic origin. Another group of zircons has a concordia age of 525.6 ± 5.3 Ma. These analyses also have variable concentrations of uranium (105–462 ppm) and thorium (34–344 ppm), with Th/U ratios ranging from 0.234 to 0.773, which also indicates their magmatic origin. The age of 245 Ma is interpreted as the crystallization age of the quartz-syenite, and the age of 525 Ma is interpreted as the age of inherited zircon.

4.1.4. Granodiorite (TK264)

Zircon grains from sample TK264 are euhedral to subhedral, ranging from 50 μm to 200 μm in length, with length to width ratios between 1:1 and 3:1. Euhedral concentric zoning is common, and some grains have inherited cores (Fig. 5). Twenty-two grains of sample TK264 were analyzed by SIMS, uranium and thorium concentrations are as follows: U = 396–1779 ppm and Th = 142–742 ppm, with Th/U ratios ranging from 0.142 to 0.546. Two analyses give relatively old ages, which may be from inherited zircons and four analyses are nearly concordant. In the concordia diagram, sixteen analyses yield a concordia age of 251.8 ± 1.9 Ma (Fig. 6e). This age is interpreted as the crystallization age of the granodiorite.

4.1.5. Granodiorite (sample TK61)

Zircon grains of the sample TK61 are mainly euhedral, ranging from 80 μm to 120 μm in length, with length to width ratios between 1:1 and 3:1. Euhedral concentric zoning is common and no inherited cores are observed (Fig. 5). Twenty three grains were analyzed by SIMS, uranium and thorium concentrations are as follows: U = 773–8198 ppm with a major population between 2000 ppm and 6000 ppm and Th = 87–6803 ppm with a major population between 800 ppm and 4000 ppm. The Th/U ratios range from 0.113 to 0.830, with a maximum between 0.4 and 0.7, which indicates a magmatic origin. Twenty analyses yield a concordia age of 256.9 ± 1.7 Ma (Fig. 6f). But these analyses have "high uranium effect", the ages become older while the uranium concentrations go higher (Li et al., 2010a). So the realistic age maybe younger than this measured age. Considering with the $^{207}Pb/^{206}Pb$ age are not affected by the uranium concentrations, the weighted mean $^{207}Pb/^{206}Pb$ age of 254.8 ± 7.6 Ma (MSWD = 0.84, Fig. 6f) is reliable and can be considered as age of granodiorite crystallization.

4.2. Zircon Hafnium–Oxygen isotope

Zircons, which are highly retentive of the magmatic oxygen isotopes, in equilibrium with mantle-derived magmas have very consistent $\delta^{18}O$ value of 5.3 ± 0.3‰ (Valley et al., 1998 and Valley et al., 2005). This value is insensitive to magmatic differentiation, because the rise of $\delta^{18}O$ in bulk rock is compensated by an increase in zircon liquid $\delta^{18}O$ fractionation from +0.5‰ for mafic melts to +1.5‰ for silicic derivatives (Valley et al., 2005). Thus $\delta^{18}O$ values in zircon above 5.6‰fingerprint an ^{18}O enriched supracrustal component in the magma from which the zircon crystallized. This component is either sedimentary rock (10–30‰) or altered volcanic rock (up to 20‰) (Eiler, 2001).

4.2.1. Pia Oac pluton (Granites, samples TK84, TK85)

Seven and sixteen in situ Hf and O isotopic analyses were carried out for zircons from the two mica leucogranite samples TK84 and Tk85, respectively (Table 3). The zircons from sample TK84 have a wide range of oxygen isotopic compositions, with $\delta^{18}O$ = 8.19‰–9.87‰ (Fig. 7a). Similarly, the zircon from sample TK85 also have a wide range of oxygen isotopic compositions, with $\delta^{18}O$ = 8.12‰–10.95‰ (Fig. 7b). For the sample TK84, the value of $^{176}Hf/^{177}Hf$ range from 0.282424 to 0.282643, the calculated ε_{Hf} (t) vary from −10.4 to −2.7 and the T_{DM}^{C} ages vary from 1330 Ma to 1744 Ma. In the sample TK85, the value of $^{176}Hf/^{177}Hf$ range from 0.282383 to 0.282564, the calculated ε_{Hf} (t) vary from −11.8 to −5.5 and the T_{DM}^{C} ages vary from 1903 Ma to 1508 Ma.

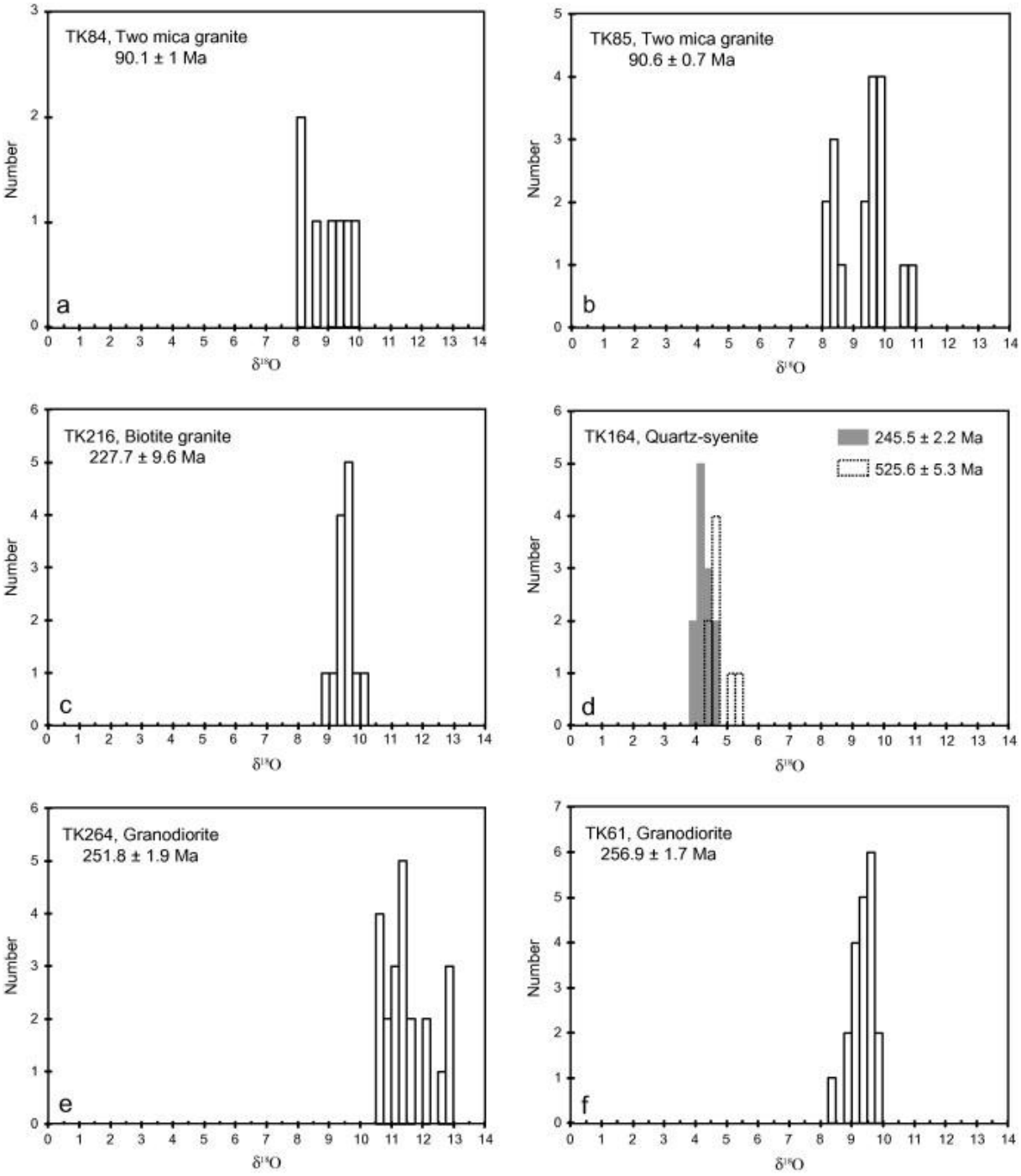

Fig. 7. : Histogram of $\delta^{18}O$ values for the analyzed northeastern Vietnam granitic rocks.

4.2.2. Bach Ha pluton (Biotite granite, sample TK216)

Thirteen in situ Hf and O isotopic analyses were carried out for zircons from the sample (TK216). The zircon have a relatively small range of Hf and O isotopes: $^{176}Hf/^{177}Hf$ = 0.282362–0.282453, ε_{Hf} (*t*) vary from −9.4 to −6.0, the calculated T_{DM}^{C} ages vary from 1869 Ma to 1666 Ma, and the value of $\delta^{18}O$ range from 8.94‰ to 10.23‰ (Fig. 7c).

4.2.3. Pia Ma pluton (Quartz-syenite, sample TK164)

Twenty in situ Hf and O isotopic analyses were carried out for zircons from the sample (TK164). Considering that this sample yields two concordia zircon SIMS U–Pb ages, the zircons from this sample can be classified into two groups. One group of zircons is ca. 245 Ma, while another group is ca. 525 Ma. Both of two groups of zircons get quite consistent O isotopic character. The value of $\delta^{18}O$ ranges from 3.99‰ to 4.74‰ (Fig. 7d) in the former group (ca. 245 Ma). The later group with the value of $\delta^{18}O$ ranges from 4.32‰ to 5.26‰ (Fig. 7d, Table 3). For the former group of zircons: $^{176}Hf/^{177}Hf$ = 0.282428–0.282576, corresponding to ε_{Hf} (t) = −6.8–(−0.2), and the calculated T_{DM}^{C} ages vary from 1712 Ma to 1289 Ma. The later group has the Hf isotopic character as follows: $^{176}Hf/^{177}Hf$ = 0.282452–0.282546, corresponding to ε_{Hf} (t) = 0.2–3.1, and the calculated T_{DM}^{C} ages vary from 1490 Ma to 1294 Ma.

4.2.4. Diem Mac pluton (Granodiorite, sample TK264)

Twenty in situ Hf and O isotopic analyses were carried out for zircons from the sample (TK264). These zircons have a relatively small range of Hf isotopes: $^{176}Hf/^{177}Hf$ = 0.282337–0.282458. The values of ε_{Hf} (t) vary from −10.0 to −7.0, the calculated T_{DM}^{C} ages vary from 1915 Ma to 1644 Ma, and the value of $\delta^{18}O$ range from 10.61‰ to 12.81‰ (Fig. 7e).

4.2.5. Cỏ Linh pluton (Granodiorite, sample TK61)

Twenty-three in situ Hf and O isotopic analyses were carried out for zircons from the sample (TK61), and the data are listed in Table 3. The zircon have a relatively small range of Hf and O isotopes: $^{176}Hf/^{177}Hf$ = 0.282473–0.282566, corresponding to ε_{Hf} (t) = −5.2–(−2.1), the calculated T_{DM}^{C} ages vary from 1618 Ma to 1417 Ma, and $\delta^{18}O$ = 8.46–9.95‰ (Fig. 7f).

4.3. Bulk-rock Sr–Nd isotope data

The initial $^{87}Sr/^{86}Sr$ (I_{Sr}) ratios and ε_{Nd} (t) values were calculated using the U–Pb zircon ages determined in this study (Table 4). We tested one sample from Late Permian to Early Triassic granodiorite (TK61) and two samples from Late Cretaceous granite (TK84, TK85). The depleted mantle model ages (T_{DM}) are reported using the model of De Paolo (1981). The two stages depleted mantle model ages (T_{DM2}) are used to reduce the error of the T_{DM}, which are caused by the Sm and Nd fractionation during the process of crustal partial remelting (Liew and Hofmann, 1988 and Li, 1996). The Cỏ Linh granodiorite (Sample TK61) yields $^{87}Rb/^{86}Sr$ and $^{87}Sr/^{86}Sr$ values of 1.61 and 0.716363, respectively. The age-corrected $^{87}Sr/^{86}Sr$ ratio is 0.7105. This rock displays $^{147}Sm/^{144}Nd$ ratio 0.0947 and the measured $^{143}Nd/^{144}Nd$ ratio 0.511959. Calculated initial ε_{Nd} (t) value is −9.7. The T_{DM} and T_{DM2} ages of sample TK61 are 1.52 Ga and 1.87 Ga, respectively. The two mica leucogranite (samples TK84 and TK85) from the Pia Oac pluton has quite similar Sr–Nd isotopic characteristics. The measured $^{87}Rb/^{86}Sr$ values of samples TK84 and TK85 are 49.5 and 47.0 while $^{87}Sr/^{86}Sr$ values are 0.788359 and 0.788476, respectively. The age-corrected $^{87}Sr/^{86}Sr$ ratios of these two samples are 0.7251 and 0.7283, respectively. These two samples display $^{147}Sm/^{144}Nd$ ratio 0.1333 and 0.1370 while the measured $^{143}Nd/^{144}Nd$ ratio are 0.512034 and 0.512061. Calculated initial ε_{Nd} (t) values are −11 and −10.5, respectively. The T_{DM} ages of samples TK84 and TK85 are 2.11 Ga and 2.15 Ga while the T_{DM2} ages of these two samples are 1.79 Ga and 1.75 Ga, respectively.

5. Discussion

5.1. Material source of NE Vietnam granitic rocks

The granitic rocks of NE Vietnam have high negative ε_{Nd} (t) values, which range from −11 to −9.7, and higher $^{87}Sr/^{86}Sr$ (0.7105–0.7283) ratios indicating crustal source (Table 4). The crustal residence age T_{DM2} values range from 1.87 Ga to 1.75 Ga. The characteristics of Nd isotope are similar to those of the Proterozoic basement of SCB (Li, 1994 and Shen et al., 1998). This suggests that ancient continental crust material was involved in the granitic rocks genesis. Almost all of the $\delta^{18}O$ values range from 8‰ to 12‰, except the Pia Ma pluton with $\delta^{18}O$ values ranging from 4.0‰ to 5.3‰ (Fig. 7d). The similarity of their geochemical features implies that they were derived from similar sources, with various degrees of differentiation. Furthermore, taking into account the zircon Lu-Hf isotope, the ε_{Hf} (t) values of zircon from the northeastern Vietnam vary from −11.8 to 3.1, implying a minor input of mantle-derived materials during the magma generation, but mostly crustal involvement. The calculated T_{DM}^{C} ages vary from 1.93 Ga to 1.33 Ga, this result is consistent with the Nd isotopic T_{DM2} ages. The TK164 sample from the Pia Ma quartz-syenite pluton shows two different isotopic characters corresponding to two groups in age (Fig. 6). The young group has negative ε_{Hf} (t) values that range from −6.8 to −0.2, and has a lower $\delta^{18}O$ value ranging from 3.99‰ to 4.74‰. The old group has positive ε_{Hf} (t) with values ranging from 0.2 to 3.1. This rock also exhibits high $\delta^{18}O$ values ranging from 4.32‰ to 5.26‰. Considering these isotopic features, we argue that this quartz-syenite originated from juvenile mantle magma during the formation and growth of continental crust then was re-melted by a young stage of magmatism. Thus our geochemical data suggest that the granitic rocks from the NE Vietnam were derived from the melting of a Proterozoic basement similar to that of the SCB (Fig. 8).

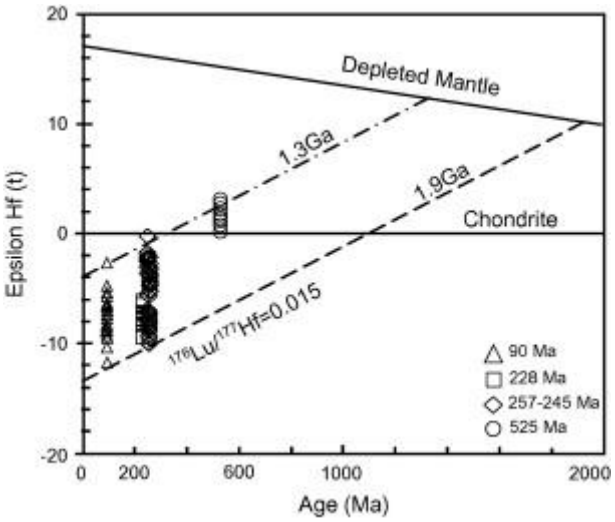

Fig. 8. : Diagram of zircon ε_{Hf} (t) isotopic composition versus ages of all zircons from northeastern Vietnam granitic rocks.

5.2. Magmatism of NE Vietnam and related tectonic significance

5.2.1. Early Paleozoic magmatism

This magmatism is well exposed in the southeast part of the SCB (Fig. 1). It is mostly distributed in the Wuyi-Baiyun-Yunkai areas (Lin et al., 2008 and reference therein). The Early Paleozoic age is also supported by the regional geology, since unmetamorphosed Late Devonian and younger sediments unconformably cover the pre-Devonian plutons and their low-grade metasedimentary host rocks (HBGMR, 1988 and JBGMR, 1984). In the present state of knowledge, the detail tectonics of the emplacement setting of these plutons is not settled yet. A crustal-thickening model was proposed because of the granites are of crustal origin (Faure et al., 2009, Charvet et al., 2010, Li et al., 2010c and Wang et al., 2011). A post-thickening extensional setting was suggested on the basis of structural observation in the Yunkai massif (Lin et al., 2008). In northeastern Vietnam, the Song Chay porphyritic granite, dated at 430–420 Ma (Fig. 2; Roger et al., 2000 and Carter et al., 2001), emplaced at the end of the Early Paleozoic orogeny. However, the intense foliation developed during the Triassic orogeny precludes any study of the syn-magmatic structures.

In NE Vietnam, as mentioned before, the quartz syenite sample (TK164) from the Pia Ma pluton yields two groups of zircon age (Fig. 3 and Fig. 6). The old group (eight grains) yields a 525.6 ± 5.3 Ma age (Fig. 6). The isotopic characteristics (Table 3) show that these grains are inherited from a juvenile mantle-derived magma during the formation of the continental crust (Fig. 7 and Fig. 8). In the SCB, such Early Paleozoic ages (ca. 530–500 Ma) are quite rare. Song et al. (2007) reported Early Paleozoic granites (520–480 Ma) in NW Yunnan province. Also, the 537 Ma to 507 Ma ages found in the Guzhai pluton in eastern Guangdong province are interpreted as those of a magmatic event (Ding et al., 2005). Several zircon grains with ages around 537 - 507 Ma are obtained in the Yunkai massif in granites yielding $^{206}Pb/^{238}U$ apparent ages 421.9 ± 9.8 Ma to 440.7 ± 5.6 Ma (Wang et al., 2007c). Chen et al. (2009a) argued for the existence of a magmatic or thermal event existent in SCB during the Cambrian time (at ca. 526 Ma). Even if we cannot completely rule out the possibility of a mixed age, our CL images support the existence of magmatic zircon around this period (Fig. 5). The significance of this magmatism is unknown. It might be related to the rifting stage experienced by the SCB from Neoproterozoic to Cambrian times (JBGMR, 1984, HBGMR, 1988 and Wang et al., 2010).

5.2.2. Late Permian-Early Triassic magmatism

In the same TK164 sample, a second zircon group yields an age around 245.5 ± 2.2 Ma. The isotopic analyses show that these zircons are due to a re-melting of the continental crust and a limited input by mantle material (Table 4; Fig. 7 and Fig. 8). From the regional geology of northeastern Vietnam, at least two magmatic episodes can be distinguished during the Triassic (Indosinian) orogeny (Tran et al., 2008 and Liu et al., 2012; Roger et al., 2012 and references therein). The earliest plutons were emplaced at ca. 280–240 Ma (Late Permian to Early Triassic), while the latest ones were emplaced at ca. 230–200 Ma (Late Triassic). Our geochronological results from samples TK61, TK164, TK264 relate to the first magmatic episode that appears as concentrated in a narrow time span, from 257 Ma to 245 Ma, with two different groups of the $\delta^{18}O$ value range from 3.99‰ to 4.74‰ and 8.4‰ to 12.8‰, respectively (Fig. 6 and Fig. 7; Table 3). The zircon Hf isotopic analyses indicate two groups of negative ε_{Hf} (t) value range from −10.0 to −7.0 and −5.0 to −2.0, respectively (Fig. 8; Table 3). The ε_{Nd} (t) value is −9.7 and $^{87}Sr/^{86}Sr$ ratio is 0.71055 (Table 4). In the NE Vietnam,

gabbro-syenite, gabbro-monzodiorite, basalt-ryholite associations and high-Al granitic rocks dated of Late Permian to Early Triassic by zircon U–Pb and biotite or amphibole $^{40}Ar/^{39}Ar$ geochronology (Fig. 3; Tran et al., 2008). The Permian alkaline magmatism is interpreted as the result of the Emeishan mantle plume (Chung and Jahn, 1995, Hanski et al., 2004, Xu et al., 2001, Xu et al., 2004 and Tran et al., 2008). The Late Permian to Early Triassic granites are also recognized in the southwestern part of the SCB (Deng et al., 2004, Ding et al., 2005, Xie et al., 2006 and Chen et al., 2011; Fig. 1).

5.2.3. Late Triassic Magmatism

In northeastern Vietnam, the Late Triassic magmatism is rarely reported (Fig. 3). Because of the "high uranium effect" (Li et al., 2010a), the TK216 sample of the undeformed biotitic granite yields $^{207}Pb/^{206}Pb$ age of 227.7 ± 9.6 Ma (Fig. 6). According to our analyses, the isotopic features of these granitic rocks show negative $\varepsilon_{Hf}(t)$ with the values ranging from −9.0 to −6.0, and $\delta^{18}O$ values ranging from 8.94‰ to 10.23‰. These data indicate the magma originated from a crustal source (Fig. 7 and Fig. 8).

In SCB, Late Triassic granitic plutons are widespread but they are related to different tectonic settings depending on their location (Fig. 1; Deng et al., 2004, Wang et al., 2007b and Chu et al., 2012). The Late Triassic granites exhibit an affinity to both S-type and *I*-type petrology (Wang et al., 2007b). Their zircon $\varepsilon_{Hf}(t)$ values range from −2.0 to −20.2 with Hf model ages of 1.2 to 2.5 Ga (Qi et al., 2007). In the Xuefengshan intracontinental belt, in the central part of the SCB, the magmatism was interpreted as a late- to post-orogenic partial melting (Chu et al., 2012). Although these plutons were related to extensional tectonics (Zhou et al., 2006, Wang et al., 2012b and Li et al., 2012), presently there is not structural data that support this view. In the northern part of the SCB, the Middle Triassic tectonics was interpreted as an extensional one developed in the southern foreland of the Dabieshan (Faure et al., 1996 and Faure et al., 1999). Triassic plutons are scattered in the SE part of the SCB, but their geodynamic significance remains unclear. In NE Vietnam, the Triassic orogeny is represented by N- to NE-vergent folds and thrust (Lepvrier et al., 2011). This orogeny is also responsible for the development of a pervasive post-solidus foliation in the Early Paleozoic plutons. The NE Vietnam Late Triassic plutons developed at the expense of a thickened continental crust. Therefore, we argue that these plutons are post-collisional bodies.

In northeastern Vietnam, the $^{40}Ar–^{39}Ar$ geochronological data of synkinematic minerals give a large span of ages from 250 Ma to 198 Ma (Fig. 9) that are interpreted as deformation age. But on the basis of our field observations, the Mesozoic deformation more likely occurred in the late Middle Triassic or early Late Triassic because the middle Triassic sedimentary succession is involved in the deformation. In the northern part of the Song Chay massif, the metamorphic rims of the igneous zircon grains yield an average $^{206}Pb/^{238}U$ age of 237 ± 15 Ma, and amphibole from a mylonitic rock yields a $^{40}Ar/^{39}Ar$ plateau age of 237 ± 4.6 Ma suggest that the main deformation occurred at ca.237 Ma (Yan et al., 2006). This age is consistent with the muscovite $^{40}Ar/^{39}Ar$ age of 236 ± 0.5 Ma from orthogneiss in the southern margin of the Song Chay massif (Maluski et al., 2001). Taking these works into account, we argue the deformation time ranges between 228 Ma and 237 Ma. Our undeformed biotitic granite, which yields a zircon SIMS U–Pb age of 227.7 ± 9.6 Ma, supports this conclusion (Fig. 9).

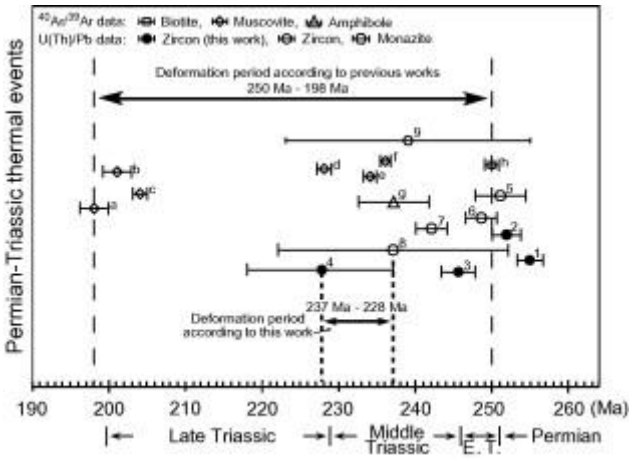

Fig. 9. : Diagram of geochronological data shows Permian-Triassic thermal events in the northeastern Vietnam. U(Th)/Pb data: 1. Granodiorite (Sample TK61); 2. Granodiorite (Sample TK264); 3. Quartz-syenite (Sample TK164); 4. Biotite granite (Sample TK216); 5. Gabbronorite (Tran et al., 2008); 6–7. Granite (Roger et al., 2012), 8. Igneous rock (Yan et al., 2006); 9. Garnet micaschist (Gilley et al., 2003). $^{40}Ar/^{39}Ar$ data: a. Marble (Maluski et al., 2001); b. Gneiss (Maluski et al., 2001); c. Micaschist (Maluski et al., 2001); d. Orthogneiss (Maluski et al., 2001); e. Micaschist (Maluski et al., 2001); f. Orthogneiss (Maluski et al., 2001); g. Mylonitic rock (Yan et al., 2006).

In the northern part of our study area, two granodiorite samples of TK61 and TK264 are dated at 255 Ma and 251 Ma, respectively. However, these rocks exhibit no or weakly developed foliation. The lack of any pervasive ductile deformation in relatively ancient granodiorite can be explained in several ways. Firstly, these plutons are located rather far away from the main syn-metamorphic thrust zone, and thus escaped the ductile deformation (Fig. 2). Secondly, these rocks contain a majority of hard-strain minerals such as hornblende and K-feldspar, therefore these plutons could be deformed with great difficulty under moderate temperature conditions (Fig. 4). Thirdly, due to the limited outcrop conditions it can be argued that our sampling sites are located in undeformed cores of these plutons whereas their rims would be more foliated. Lastly, it can also be argued that there is a very short-lived tectonic stagnancy in this period although this possibility needs further detail structural work to be tested. Along the southern margin of the SCB, the top to the N/NE deformation is well documented both in Song Chay and Yunkai massifs (Lin et al., 2008 and Lepvrier et al., 2011). The Triassic deformation ages also cluster between 250 Ma and 200 Ma (Wang et al., 2005, Wang et al., 2007a, Cai and Zhang, 2009 and Zhang et al., 2011). The central part of the Yunkai massif, and its northern thrust zone, yield metamorphic minerals dated at 230–208 Ma by the $^{40}Ar–^{39}Ar$ method (Wang et al., 2007a). This deformation phase is considered as the main ductile one in the Yunkai massif (Lin et al., 2008). At the regional scale, a similar ductile deformation has been recognized in the Song Chay orthogneiss, and its metamorphic country rocks (Roger et al., 2000, Maluski et al., 2001, Yan et al., 2006 and Lepvrier et al., 2011). According to Lepvrier et al. (2011), the SCB subducted to the South beneath the Day Nui Con Voi massif along the Song Chay suture during the Late Permian to Middle Triassic time. The top-to-the-NE/N deformation along the south margin of SCB is interpreted as the thrusting of the continental crust of the subducted plate.

5.2.4. The Late Cretaceous magmatism (ca. 95–85 Ma)

In NE Vietnam, the granitic samples TK84 and TK85, dated around 90 Ma, have high SiO_2 value (72.02–74.31%), and the A/CNK value varies from 1.16 to 1.45 (Wang et al., 2011; our unpublished data). The initial $^{87}Sr/^{86}Sr$ ratio ranges from 0.7251 to 0.7283, the value of $\delta^{18}O$ ranges from 8.17‰ to 10.95‰ and the values of ε_{Hf} (t) vary from −11.7 to −2.7 (Fig. 7 and Fig. 8). These geochemical features show that the Late Cretaceous granitic plutons of NE Vietnam are derived from a crustal source. The Late Cretaceous granitic rocks are also distributed in the southwestern and southeastern parts of the SCB (Fig. 1). The geochemical features of the Late Cretaceous granites are reported as high-K calc-alkaline *I*-type granites, as well as *A*-type granites, highly differentiated I- type granites and I- and A- type complexes (Dong and Peng, 1994 and Martin et al., 1994; Chen and Jahn, 1998, Chen et al., 2000, Zhou et al., 2006, Qiu et al., 2008 and He et al., 2011). The magmatism occurred in the back-arc extensional tectonic setting (Li, 2000, Jiang et al., 2011 and He et al., 2011). During the Late Cretaceous, the eastern part of SCB underwent lithospheric thinning coeval with an asthenospheric mantle upwelling that triggered mafic melt underplating (Li, 2000 and Yan et al., 2005). The geochemical features of the Late Cretaceous granites of NE Vietnam are similar to the Late Cretaceous S-type granite reported in southwest China (Cheng and Mao, 2010; and references therein). We suggest that the granitic rocks of this period in NE Vietnam were derived from the melting of continental crust.

Our geochronological and isotopic data show that the characteristics of magmatism in NE Vietnam are similar to South China block, especially in the southern margin of SCB. The stratigraphic sequence and bulk architecture of northeastern Vietnam and Chinese Guangxi provinces are comparable (Fig. 2; Table 1; Lepvrier et al., 2011). Furthermore, the Permo-Triassic kinematics in NE Vietnam belt is also comparable to the Yunkai massif in the southern margin of SCB (Lin et al., 2008 and Lepvrier et al., 2011). Therefore, we argue that northeastern Vietnam is geologically part of the South China block. In the south margin of SCB (such as Chinese Yunnan and Guangxi provinces) and NE Vietnam, the gabbro, pillow basalts, mafic dykes cropping out have been considered as the “Babu ophiolites” (Cai and Zhang, 2009). The observations near Cao Bang show that the mafic rocks are olistoliths reworked in the Middle Triassic turbidite, as observed in Guangxi province, the gabbro intrudes the Late Paleozoic host rocks with a thermal metamorphism (Faure et al., submitted for publication). Thus these rocks did not form an ophiolitic suite but rather were emplaced in an intraplate setting related to the Emeishan plume (Tran et al., 2008). Though still speculated, an ophiolitic suture between NE Vietnam and South China appears unlikely there, as the suture zone is located along the Song Chay mélange.

6. Conclusion

The application of zircon U–Pb geochronology and isotopic investigation, allow us to draw the following conclusions:

Zircon SIMS dating indicates that at least four thermal events occurred in the NE Vietnam: at ca. 525 Ma, at ca.254 Ma to 251 Ma, at ca.245–220 Ma, and at ca.91 Ma. The Early Paleozoic (525 Ma) thermal event has positive ε_{Hf} (t) values ranging from 0.2 to 3.1 and $\delta^{18}O$ value ranging from 4.32‰ to 5.26‰. This event might be related to the rifting experienced by the SCB in Neoproterozoic to Cambrian periods.

The Late Permian to Early Triassic (254 Ma to 245 Ma) granitoids show zircon ε_{Hf} (t) ranging from −10 to −2.0, and $\delta^{18}O$ value ranging from 8.46‰ to 12.81‰. These features indicate crustal source for the granitic magma and limited input by mantle material. This magmatism is possibly related to the intraplate Emeishan magmatism. However, a regional extensional setting in the southern part of SCB cannot be discarded.

The Late Triassic (230–200 Ma) granitic rocks have negative ε_{Hf} (t) values ranging from −9.0 to −6.4, and $\delta^{18}O$ value ranging from 8.94‰ to 10.23‰. The isotopic characters show these granitic rocks are also derived from a crustal source and represent post-orogenic plutons.

The Late Cretaceous granites (ca.90 Ma) are *S*-type granites and are derived from the melting of continental crust.

Our Sr–Nd–Hf–O isotopic data suggest that the NE Vietnam granitoid magmas formed by partial melting of a Paleoproterozoic crust with minor input from mantle-derived material. Because of the poor outcrop and small size of these granitoid plutons, systematic geochemical works are still rare. Further works of integrated geochemistry and detail structural analyses are needed in order to substantiate the geological evolution of this part of the SCB.

Acknowledgements

Field and laboratory expenses have been funded by National Natural Science Foundation of China (41225009), Chinese National 973 Project (2009CB825008), the Innovative Project of the Chinese Academy of Sciences (Grant No. KZCX1-YW-15-1), and the Major National Science and Technology Project (No. 2011ZX05008-001). We thank Saihong Yang for help with zircon CL imaging, Qiuli Li, Wenbin Ji, Guoqiang Tang and Yu Liu for help with zircon U/Pb analysis, and Yue-Heng Yang for help with zircon Hf analysis.

References

Bourret, 1922
R. Bourret
Les Nappes dans le Nord-Est du Tonkin. Comptes Rendus de l'Académie des Sciences – Series IIA
Earth and Planetary Science, 174 (1922), pp. 406–408

Cai and Zhang, 2009
J.X. Cai, K.J. Zhang
A new model for the Indochina and South China collision during the late permian to the middle triassic original research article
Tectonophysics, 467 (2009), pp. 35–43

Cai et al., 2006
M.H. Cai, L.Q. He, G.Q. Liu
SHRIMP zircon U–Pb dating of the intrusive rocks in the Dachang tin-polymetallic ore district, Guangxi and their geological significance
Geological Review, 52 (2006), pp. 409–414 (in Chinese with English abstract)

Carter et al., 2001
A. Carter, D. Roques, C. Bristow, P. Kinny

Understanding Mesozoic accretion in Southeast Asia: signigicance of Triassic thermotectonism (Indosinian orogeny) in Vietnam
Geology, 29 (2001), pp. 211–214

Charvet et al., 1994
J. Charvet, H. Lapierre, Y. Yu
Geodynamics significance of the Mesozoic volcanism of southeastern China
Journal of Southeast Asian Earth Sciences, 9 (1994), pp. 387–396

Charvet et al., 2010
J. Charvet, L. Shu, M. Faure, F. Choulet, B. Wang, H. Lu, N.L. Breton
Structural development of the Lower Paleozoic belt of South China: genesis of an intracontinental orogen
Journal of Asian Earth Sciences, 39 (2010), pp. 309–330

Chen, 1999
A. Chen
Mirror-image thrusting in the South China Orogentic Belt: tectonic evidence from western Fujian, southeastern China
Tectonophysics, 305 (1999), pp. 497–519

Chen and Jahn, 1998
J.F. Chen, B.M. Jahn
Crustal evolution of southeastern China: Nd and Sr isotopic evidence
Tectonophysics, 284 (1998), pp. 101–133

Chen and Zhu, 1993
Y.C. Chen, Y.S. Zhu
Mineral Deposits of China
Geological Publishing House, Beijing (1993) pp. 209–211 (in Chinese)

Chen et al., 2000
C.H. Chen, W. Lin, C.Y. Lee, J.L. Tien, H.Y. Lu, Y.H. Lai
Cretaceous fractionated *I*-type granitoids and metaluminous *A*-type granites in SE China: the Late Yanshanian post-orogenic magmatism
Transaction Royal Society of Edinburgh, Earth Science, 91 (2000), pp. 195–205

Chen et al., 2008
Chen, M.H., Cheng, Y.B., Zhang, W., Yang, Z.X., Lu, G., 2008. Primary Study on the Relationship between Yanshanian Magma Activity and Mineralization in Youjiang folded belt. In: Chen, Y.C., Xue, C.J., Zhang, C.Q. (Eds.), Main Attacking Deep, Pushing Forward Western and Scanning the World. 9th National Deposit Meeting. Geological Publishing House, Beijing, pp. 241–242 (in Chinese).

Chen et al., 2009a
D.Z. Chen, J.G. Wang, H.R. Qing, D.T. Yan, R.W. Li
Hydrothermal venting activities in the Early Cambrian, South China: petrological, geochronological and stable isotopic constraints
Chemical Geology, 258 (2009), pp. 168–181

Chen et al., 2009b

M.H. Chen, J.W. Mao, W. Zhang, Z.X. Yang, G. Lu, K.J. Hou, J.H. Liu
Zircon U–Pb age and Hf isotopic composition of the Baiceng ultrabasic rock veins in Zhenfeng county, southwestern Guizhou Province, China
Mineral Deposits, 28 (2009), pp. 240–250 (in Chinese with English abstract)

Chen et al., 2011
C.H. Chen, P.S. Hsieh, C.Y. Lee, H.W. Zhou
Two episodes of the Indosinian thermal event on the South China Block: constraints from LA-ICPMS U–Pb zircon and electron microprobe monazite ages of the Darongshan S-type granitic suite
Gondwana Research, 19 (2011), pp. 1008–1023

Cheng and Mao, 2010
Y.B. Cheng, J.W. Mao
Age and geochemistry of granites in Gejiu area, Yunnan province, SW China: constraints on their petrogenesis and tectonic setting
Lithos, 120 (2010), pp. 258–276

Chu and Lin, this volume
Chu, Y., Lin, W., this volume. Phanerozoic polyorogenic deformation in southern Jiuling massif, northern South China block: constraints from structural analysis and geochronology. Journal of Asian Earth Sciences, in press.

Chu et al., 2002
N.C. Chu, R.N. Taylor, V. Chavagnac, R.W. Nesbitt, R.M. Boella, J.A. Milton, C.R. German, G. Bayon, K. Burton
Hf isotope ratio analysis using multi-collector inductively coupled plasma mass spectrometry: an evaluation of isobaric interference corrections
Journal of Analytical Atomic Spectrometry, 17 (2002), pp. 1567–1574

Chu et al., 2012
Y. Chu, W. Lin, M. Faure, Q.C. Wang, W.B. Ji
Phanerozoic tectonothermal events of the Xuefengshan Belt, central South China: Implications from U–Pb age and Lu–Hf determinations of granites
Lithos, 150 (2012), pp. 243–255

Chung and Jahn, 1995
S.L. Chung, B.M. Jahn
Plume-lithosphere interaction in generation of the Emeishanflood basalts at the Permian–Triassic boundary
Geology, 10 (1995), pp. 889–892

De Paolo, 1981
D.J. De Paolo
A neodymium and strontium isotopic study of the Mesozoic calcalkaline granitic batholiths of the Sierra Nevada and Peninsular Ranges, California
Journal of Geophysical Research, 86 (1981), pp. 10470–10488

Deng et al., 2004
X.G. Deng, Z.G. Chen, X.H. Li, D.Y. Liu

SHRIMP U–Pb zircon dating of the Darongshan-Shiwandashan granitoid belt in southeastern Guangxi, China
Geological Review, 50 (2004), pp. 427–432 (in Chinese with English abstract)

Deprat, 1915
Deprat, J., 1915. Etude géologique de la région septentrionale du haut Tonkin (feuille de Pa Kha, Ha Giang, Ma Li Po, Yen Minh). Mémoire du Service Géologique de l'Indochine, Hanoi, vol. IV, 174pp.

Ding et al., 2005
X. Ding, X.M. Zhou, T. Sun
The episodic growth of the continental crustal basement in South Chian: single zircon LA-ICPMS U–Pb dating of Guzhai granodiorite in Guangdong
Geological Review, 51 (2005), pp. 382–392

Dong and Peng, 1994
C.W. Dong, Y.M. Peng
Qingtian composite body-the coexisting of two different types of granties
Journal Zhejiang University (Natural Science), 28 (1994), pp. 440–448 (in Chinese with English abstract)

Eiler, 2001
J.M. Eiler
Oxygen isotope variations of basaltic lavas and upper mantle rocks
Reviews in Mineralogy and Geochemistry, 43 (2001), pp. 319–364

Faure et al., 1996
M. Faure, Y. Sun, L. Shu, P. Monié, J. Charvet
Extensional tectonics within a subduction type orogen: the case study of the Wugongshan dome (Jiangxi Province, southeastern China)
Tectonophysics, 263 (1996), pp. 77–106

Faure et al., 1999
M. Faure, W. Lin, L.S. Shu, Y. Sun, U. Schärer
Tectonics of the Dabieshan (eastern China) and possible exhumation mechanism of ultra high-pressure rocks
Terra Nova, 11 (1999), pp. 251–258

Faure et al., 2009
M. Faure, L. Shu, B. Wang, J. Charvet, F. Choulet, P. Monié
Intracontinental subduction: a possible mechanism for the Early Palaeozoic Orogen of SE China
Terra Nova, 21 (2009), pp. 360–368

Faure et al., submitted for publication
Faure, M., Lepvrier, C., Nguyen, V.V., Vu, V.T., Lin, W., Chen, Z.C., submitted for publication. The South China Block-Indochina collision: where, when, and how? Journal of Asian Earth Sciences.

FBGMR, 1985

FBGMR (Fujian Bureau of Geology and Mineral Resources), 1985. Regional Geology of Fujian Province. Geological Publishing House, Beijing, pp. 671.

Fromaget, 1941
J. Fromaget
L'Indochine francaise, sa structure géologique, ses roches, ses mines et leurs relations possibles avec la tectonique
Bulletin Service Géologique de l'Indochine, 26 (1941), pp. 1–140

GDBGMR, 1982
GDBGMR (Guangdong Bureau of Geology and Mineral Resources), 1982. Regional Geology of Guangdong Province. Geological Publishing House, Beijing, pp. 941.

Gilder et al., 1991
S. Gilder, G.R. Keller, M. Luo
Eastern Asia and the western Pacific timing and spatial distribution of rifting in China
Tectonophysics, 197 (1991), pp. 225–243

Gilley et al., 2003
L.D. Gilley, T.M. Harrison, P.H. Leloup, F.J. Ryerson, O.M. Lovera, J.H. Wang
Direct dating of left-lateral deformation along the Red River shear zone, China and Vietnam
Journal of Geophysical Research, 108 (B2) (2003), p. 2127
doi:10.1029/2001JB001726

GXBGMR, 1982
GXBGMR (Guangxi Bureau of Geology and Mineral Resources), 1982. Regional Geology of Guangdong Province. Geological Publishing House, Beijing, pp. 853.

Hacker et al., 1998
B. Hacker, L. Ratschbacher, L. Webb, T. Ireland, D. Walker, S.W. Dong
U–Pb zircon ages constrain the architecture of the ultrahigh-pressure Qinling-Dabie Orogen, China
Earth and Planetary Science Letters, 161 (1998), pp. 215–230

Hanski et al., 2004
E. Hanski, R.J. Walker, H. Huhma, G.V. Polyakov, P.A. Balykin, T.H. Tran, T.P. Ngo
Origin of the Permian-Triassic komatiites, northwestern Vietnam
Contributions to Mineralogy and Petrology, 147 (2004), pp. 453–469

HBGMR, 1988
HBGMR (Hunan Bureau of Geology and Mineral Resources), 1988. Regional Geology of Hunan Province. Geological Publishing House, Beijing, pp. 726.

He et al., 2011
Z.Y. He, X.S. Xu, Y.L. Niu
Petrogenesis and tectonic significance of a Mesozoic granite–syenite–gabbro association from inland South China

Lithos, 119 (2011), pp. 621–641

Hou et al., 2007
Z.Q. Hou, K. Zaw, G.T. Pan, X.X. Mo, Q. Xu, Y.Z. Hu, X.Z. Li
Sanjiang Tethyan metallogenesis in S.W. China: tectonic setting, metallogenic epochs and deposit types
Ore Geology Reviews, 31 (2007), pp. 48–87

Huang, 1978
T.K. Huang
An outline of the tectonic characteristics of China
Ecologae Geologicae Helvetiae, 71 (1978), pp. 611–635

Huang et al., 1980
J.Q. Huang, J.S. Ren, C.F. Jiang, Z.K. Zhang, D.Y. Qin
Tectonics and Evolution of China
Science Press House, Beijing (1980) pp. 124 (in Chinese)

JBGMR, 1984
JBGMR (Jiangxi Bureau of Geology and Mineral Resources), 1984, Regional geology of Jiangxi Province. Geological Publishing House, Beijing, pp. 921.

Jian et al., 1999
P. Jian, X.F. Wang, L.Q. He, C.S. Wang
U–Pb zircon dating of anothosite and plagiogranite from the Jinshaj iang ophiolite belt
Acta Petrologica Sinica, 15 (1999), pp. 590–593

Jian et al., 2003
P. Jian, D.Y. Liu, X.M. Sun
SHRIMP Dating of Baimaxueshan and Ludian Granitoid Batholiths, Northwestern Yunnan Province, and Its Geological Implications
Acta Geoscientia Sinica, 24 (2003), pp. 337–342

Jiang et al., 2011
Y.H. Jiang, P. Zhao, Q. Zhou, S.Y. Liao, G.D. Jin
Petrogenesis and tectonic implications of Early Cretaceous *S*- and *A*-type granites in the northwest of the Gan-Hang rift, SE China
Lithos, 121 (2011), pp. 55–73

John et al., 1990
B.M. Jahn, X.H. Zhou, J.L. Li
Formation and tectonic evolution of southeastern China and Taiwan: isotopic and geochemical constraints
Tectonophysics, 183 (1990), pp. 145–160

Lan et al., 2003
C.Y. Lan, S.L. Chung, V.L. Trinh, C.H. Lo, T.Y. Lee, S.A. Mertzman, J. Shen
Geochemical and Sr–Nd isotopic constraints from the Kontum massif, central Vietnam on the crustal evolution of the Indochina block
Precambrian Research, 122 (2003), pp. 7–27

Leech and Webb, 2012
M.L. Leech, L.E. Webb
Is the HP-UHP Hong'an-Dabie-Sulu orogen a piercing point for offset on the Tan-Lu fault?
Journal of Asian Earth Sciences, 63 (2012), pp. 112–129

Leloup et al., 1995
P.H. Leloup, R. Lacassin, P. Tapponnier, U. Schärer, D.L. Zhong, X.H. Liu, L.S. Zhang, S.C. Ji, T.T. Phan
The Ailo Shan-Red River shear zone (Yunnan, China), Tertiary transform boundary of Indochina
Tectonophysics, 252 (1995), pp. 3–84

Lepvrier et al., 1997
C. Lepvrier, H. Maluski, V.V. Nguyen, D. Roques, V. Axente, G. Rangin
Indosinian NW-trending shear zones within the Truong Son belt (Vietnam)
Tectonophysics, 283 (1997), pp. 105–127

Lepvrier et al., 2004
C. Lepvrier, H. Maluski, V.T. Vu, A. Leyreloup, T.T. Phan, V.V. Nguyen
The Early Triassic Indosinian orogeny in Vietnam (Truong Son Belt and Kontum Massif): implications for the geodynamic evolution of Indochina
Tectonophysics, 393 (2004), pp. 87–118

Lepvrier et al., 2008
C. Lepvrier, V.V. Nguyen, H. Maluski, T.T. Phan, V.T. Vu
Indosinian tectonics in Vietnam
Comptes Rendus Geosciences, 340 (2008), pp. 94–111

Lepvrier et al., 2011
C. Lepvrier, M. Faure, V.V. Nguyen, V.T. Vu, W. Lin, T.T. Ta, H.P. Ta
North-directed Triassic nappes in Northeastern Vietnam (East Bac Bo)
Journal of Asian Earth Sciences, 41 (2011), pp. 56–68

Li, 1994
X. Li
A comprehensive U/Pb, Sm/Nd, Rb/Sr and $^{40}Ar/^{39}Ar$ geochronological study on Guidong granodiorite, southeast China: records of multiple tectonothermal events in a single pluton
Chemical Geology, 115 (1994), pp. 283–295

Li, 1996
X.H. Li
A discussion on the model and isochron ages of Sm-Nd isotopic systematics: suitability and limitation

Scientia Geologica Sinica, 31 (1996), pp. 97–104

Li, 1999
X.H. Li
U–Pb zircon ages of granites from the southern margin of the Yangtze margin: Timing of Neoproterozoic Jinning Orogen in SE China and implication for Rodinia assembly
Precambrian Research, 97 (1999), pp. 43–57

Li, 2000
X.H. Li
Cretaceous magmatism and lithosphere extension in Southeast China
Jounranl of Asian Earth Sciences, 18 (2000), pp. 293–305

Li and Li, 2007
Z.X. Li, X.H. Li
Formation of the 1300 km wide intracontinental orogen and postorogenic magmatic province in Mesozoic south China: a flat-slab subduction model
Geology, 35 (2007), pp. 179–182

Li et al., 2001
J.W. Li, M.F. Zhou, X.F. Li, Z.R. Fu, Z.J. Li
The Hunan-Jiangxi strike-slip fault system in southern China: Southern termination of the Tan-Lu fault
Journal of Geodynamics, 32 (2001), pp. 333–354

Li et al., 2004
Li, X.H., Chung, S.L., Zhou, H.W., Lo, C.H., Liu, Y., Chen, C.H., 2004. Jurassic intraplate magmatism in southern Hunan-eastern Guangxi: $^{40}Ar/^{39}Ar$ dating, geochemistry, Sr–Nd isotopes and implications for tectonic evolution of SE China. In: Malpas, J., Fletcher, C.J., Aitchison, J.C., Ali, J. (Eds.), Aspects of the Tectonic Evolution of China. Geological Society of London. Special Publication, vol. 226, pp. 193–216.

Li et al., 2006
X.H. Li, Z.X. Li, W.X. Li, Y.J. Wang
Initiation of the Indosinian Orogeny in South China: evidence for a Permian magmatic arc on Hainan Island
Journal of Geology, 114 (2006), pp. 341–353

Li et al., 2009a
X.H. Li, W.X. Li, Z.X. Li, C.H. Lo, J. Wang, M.F. Ye, Y.H. Yang
Amalgamation between the Yangtze and Cathaysia Blocks in South China: constraints from SHRIMP U–Pb zircon ages, geochemistry and Nd–Hf isotopes of the Shuangxiwu volcanic rocks
Precambrian Research, 174 (2009), pp. 117–128

Li et al., 2009b
X.H. Li, Y. Liu, Q.L. Li, C.H. Guo, K.R. Chamberlain

Precise determination of Phanerozoic zircon Pb/Pb age by multicollector SIMS without external standardization
Geochemistry, Geophysics, Geosystems, 10 (2009), p. Q04010
http://dx.doi.org/10.1029/2009GC002400

Li et al., 2010a
Q.L. Li, X.H. Li, Y. Liu, G.Q. Tang, J.H. Yang, W.G. Zhu
Precise U–Pb and Pb–Pb dating of Phanerozoic baddeleyite by SIMS with oxygen flooding technique
Journal of Analytical Atomic Spectrometry, 25 (2010), pp. 1107–1113

Li et al., 2010b
Q.L. Li, X.H. Li, Y. Liu, F.Y. Wu, J.H. Yang, R.H. Mitchell
Precise U–Pb and Th–Pb age determination of kimberlitic perovskites by secondary ion mass spectrometry
Chemical Geology, 269 (2010), pp. 396–405

Li et al., 2010c
X.H. Li, W.G. Long, Q.L. Li, Y. Liu, Y.F. Zheng, Y.H. Yang, K.R. Chamberlain, D.F. Wan, C.H. Guo, X.C. Wang, H. Tao
Penglai zircon megacrysts: a potential new working reference material for microbeam determination of Hf–O isotopes and U–Pb age
Geostandards and Geoanalytical Research, 34 (2010), pp. 117–134

Li et al., 2010d
Z.X. Li, X.H. Li, J.A. Wartho, C. Clark, W.X. Li, C.L. Zhang, C. Bao
Magmatic and metamorphic events during the early Paleozoic Wuyi-Yunkai orogeny, southeastern South China: new age constraints and pressure-temperature conditions
Geologyical Society of America Bulletin, 122 (2010), pp. 772–793

Li et al., 2012
W. Li, C. Ma, Y. Liu, P. Robinson
Discovery of the Indosinian aluminum *A*-type granite in Zhejiang Province and its geological significance
Science China Earth Sciences, 55 (2012), pp. 13–25

Liang et al., 2008
T. Liang, Y.C. Chen, D.H. Wang, M.H. Cai
Geology and Geochemistry of the Dachang Tin Polymetallic Deposit, Guangxi ProvinceGeological Publishing House, Beijing (2008) pp. 1–229 (in Chinese)

Liew and Hofmann, 1988
T.C. Liew, A.W. Hofmann
Precambrian crustal components, plutonic assimilations, plate environment of the Hercynian fold belt of central Europe: indications from a Nd and Sr isotopic study
Contributions to Mineralogy and Petrology, 98 (1988), pp. 129–138

Lin et al., 2000
W. Lin, M. Faure, P. Monié, U. Schäerer, L. Zhang, Y. Sun

Tectonics of SE China: new insights from the Lushan massif (Jiangxi Province)
Tectonics, 19 (2000), pp. 852–871

Lin et al., 2008
W. Lin, Q.C. Wang, K. Chen
Phanerozoic tectonics of south China block: new insights from the polyphase deformation in the Yunkai massif
Tectonics, 27 (2008), p. TC6004 doi:10.1029/2007TC002207

Lin et al., 2011
W. Lin, M. Faure, C. Lepvrier, Z.C. Chen, Y. Chu, Q.C. Wang, V.V. Nguyen, V.T. Vu
The Early Mesozoic thrust and folds sheet structure along the southern margin of South China Block and its geodynamic
Scientia Geologica Sinica, 46 (2011), pp. 134–145 (in Chinese with English abstract)

Liu et al., 2007
Y.P. Liu, Z.X. Li, H.M. Li
U–Pb geochronology of cassiterite and zircon from the Dulong Sn–Zn deposit: evidence for Cretaceous large—scale granitic magmatism and mineralization events in southeastern Yunnan province, China
Acta Petrologica Sinica, 23 (2007), pp. 967–976 (in Chinese with English abstract)

Liu et al., 2010
S. Liu, W.C. Su, R.Z. Hu, C.X. Feng, S. Gao, I.M. Coulson, T. Wang, G.Y. Feng, Y. Tao, Y. Xia
Geochronological and geochemical constraints on the petrogenesis of alkaline ultramafic dykes from southwest Guizhou Province, SW China
Lithos, 114 (2010), pp. 253–264

Liu et al., 2012
J.L. Liu, M.D. Tran, Y. Tang, Q.L. Nguyen, T.H. Tran, W.B. Wu, J.F. Chen, Z.C. Zhang, Z.D. Zhao
Permo-Triassic granitoids in the northern part of the Truong Son belt, NW Vietnam: Geochronology, geochemistry and tectonic implications
Gondwana Research, 22 (2012), pp. 628–644

Ludwig, 2001
Ludwig, K.R., 2001. Users manual for Isoplot/Ex rev. 2.49. Berkeley Geochronology Centre Special, Publication. No. 1a, pp. 56.

Lugmair and Marti, 1978
G.W. Lugmair, K. Marti
Lunar initial $^{143}Nd/^{144}Nd$: differential evolution of the lunar crust and mantle
Earth and Planetary Science Letters, 39 (1978), pp. 349–357

Maluski et al., 2001
H. Maluski, C. Lepvrierb, L. Jolivetb, A. Carterc, D. Roquesc, O. Beyssacd
Ar–Ar and fission-track ages in the Song Chay Massif: early Triassic and Cenozoic tectonics in northern Vietnam
Journal of Asian Earth Sciences, 19 (2001), pp. 233–248

Martin et al., 1994
H. Martin, B. Bonin, R. Capdevila, B.M. Jahn, J. Lameyre, Y. Wang
The Kuiqi peralkaline granitic complex (SE China): petrology and geochemistry
Journal of Petrology, 35 (1994), pp. 983–1015

Metcalfe, 2002
I. Metcalfe
Permian tectonic framework and palaeogeography of SE Asia
Journal of Asian Earth Science, 20 (2002), pp. 551–566

Nagy et al., 2001
E.A. Nagy, H. Maluski, C. Lepvrier, U. Schärer, T.T. Phan, A. Leyreloup, V.T. Vu
Geodynamic significance of the Kontum massif in central Vietnam: composite $^{40}Ar/^{39}Ar$ and U–Pb ages from Paleozoic to Triassic
Journal of Geology, 109 (2001), pp. 755–770

Nakano et al., 2008
N. Nakano, Y. Osanai, T.M. Nguyen, T. Miyamoto, Y. Hayasaka, M. Owada
Discovery of high-pressure granulite-facies metamorphism in northern Vietnam: constraints on the Permo-Triassic Indochinese continental collision tectonics
Comptes Rendus Geosciences, 340 (2008), pp. 127–139

Osanai et al., 2001
Y. Osanai, M. Owada, T. Tsunogae, T. Toyoshima, T. Hokada, V.L. Trinh, K. Sajeev, N. Nakano
Ultra high-temperature pelitic granulites from Kontum massif, central Vietnam: evidence for East Asian juxtaposition at ca.250 Ma
Gondwana Research, 4 (2001), pp. 720–723

Osanai et al., 2006
Y. Osanai, M. Owada, A. Kamei, T. Hamamto, H. Kagami, T. Toyoshima, H. Nakano, N.N. Tran
The Higo metamorphic complex in Kyushu, Japan as the fragment of Permo-Triassic metamorphic complexes in East Asia
Gondwana Research, 9 (2006), pp. 152–166

Phan et al., 2012
T.T. Phan, V.L. Ngo, V.H. Nguyen, Q.V. Hoang, V.T. Bui, T.T. Bui, T.T. Mai, H. Nguyen
Late Quaternary tectonics and seismotectonics along the Red River fault zone, North Vietnam
Earth-Science Reviews, 114 (2012), pp. 224–235

Qi et al., 2007
C.S. Qi, X.G. Deng, W.X. Li, X.H. Li, Y.H. Yang, L.W. Xie
Origin of the Darongshan-Shiwandashan *S*-type granitoid belt from southeastern Guangxi: geochemicaland Sr–Nd–Hf isotopic constraints
Acta Petrologica Sinica, 2 (2007), pp. 403–412

Qiu et al., 2008
J.S. Qiu, E. Xiao, J. Hu, X.S. Xu, S.Y. Jiang, Z. Li
Petrogenesis of highly fractionated I-type granites in the coastal area of northeastern Fujian Province: constraints from zircon U–Pb geochronology, geochemistry and Nd–Hf isotopes
Acta Petrologica Sinica, 24 (2008), pp. 2468–2484

Roger et al., 2000
F. Roger, P.H. Leloup, M. Jolivet, R. Lacassin, T.T. Phan, M. Brunel, D. Seward
Long and complex thermal history of the Song Chay metamorphic dome (Northern Vietnam) by multi-system geochronology
Tectonophysics, 321 (2000), pp. 449–466

Roger et al., 2010
F. Roger, M. Jolivet, J. Malavieille
The tectonic evolution of the Songpan-Garze (North Tibet) and adjacent areas from Proterozoic to Present: a synthesis
Journal of Asian Earth Sciences, 39 (2010), pp. 254–269

Roger et al., 2012
F. Roger, H. Maluski, C. Lepvrier, V.T. Vu, J.L. Paquette
LA-ICPMS zircons U/Pb dating of Permo-Triassic and Cretaceous magmatisms in Northern Vietnam-Geodynamical implication
Journal of Asian Earth Sciences, 48 (2012), pp. 72–82

Sengör et al., 1988
A.M.C. Sengör, D. Altiner, A. Cin, T. Ustaomer, K.J. Hsu
Origin and assembly of the Tethyside orogenic collage at the expense of Gondwana Land
Geological Society Special Publication, 37 (1988), pp. 119–181

Shen et al., 1998
W.Z. Shen, H.F. Ling, W.X. Li, D.Z. Wang
Sr and Nd isotope of Mesozoic granitoids in Jiangxi Province
Chinese Science Bulletin, 43 (1998), pp. 2653–2657

Shu et al., 1994
L. Shu, G. Zhou, Y. Shi, J. Yin
A study on the high pressure metamorphic blueschist and its late Proterozoic age in the Eastern Jiangnan belt
Chinese Science Bulletin, 39 (1994), pp. 1200–1204

Shu et al., 2008a
L.S. Shu, M. Faure, B. Wang, X.M. Zhou, B. Song
Late Palaeozoic-Early Mesozoic geological features of South China: response to the Indosinian collision events in Southeast Asia
Comptes Rendus Geosciences, 340 (2008), pp. 151–165

Shu et al., 2008b
L.S. Shu, J.H. Yu, D. Jia, B. Wang, W. Shen, Y.Q. Zhang
Early Palaeozoic orogenic belt in the eastern segment of South China

Geological Bulletin of China, 27 (2008), pp. 1581–1593

Shui, 1987
T. Shui
Tectonic framework of the continental basement of southeast China
Scientia Sinica (B), 31 (1987), pp. 24–34 (in Chinese)

Sláma et al., 2008
J. Sláma, J. Košler, D.J. Condon, J.L. Crowley, A. Gerdes, J.M. Hanchar, M.S.A. Horstwood, G.A. Morris, L. Nasdala, N. Norberg, U. Schaltegger, B. Schoene, M.N. Tubrett, M.J. Whitehouse
Plešovice zircon – a new natural reference material for U–Pb and Hf isotopic microanalysis
Chemical Geology, 249 (2008), pp. 1–35

Söderlund et al., 2004
U. Söderlund, P.J. Patchett, J.D. Vervoort, C.E. Isachsen
The ^{176}Lu decay constant determined by Lu–Hf and U–Pb isotope systematics of Precambrian mafic intrusions
Earth and Planetary Science Letters, 219 (2004), pp. 311–324

Sone and Metcalfe, 2008
M. Sone, I. Metcalfe
Parallel Tethyan sutures in mainland Southeast Asia: new insights for Palaeo-Tethys closure and implications for the Indosinian orogeny
Comptes Rendus Geoscience, 340 (2008), pp. 166–179

Song et al., 2007
S. Song, J. Ji, C. Wei, L. Su, Y. Zheng, B. Song, L. Zhang
Early Paleozoic granite in Nujiang River of northwest Yunnan in southwestern China and its tectonic implications
Chinese Science Bulletin, 52 (2007), pp. 2402–2406

Stacey and Kramers, 1975
J.S. Stacey, J.D. Kramers
Approximation of terrestrial lead isotope evolution by a two-stage model
Earth and Planetary Science Letters, 26 (1975), pp. 207–221

Steiger and Jäger, 1977
R.H. Steiger, E. Jäger
Subcommission on geochronology; convention on the use of decay constants in geochronology and cosmochronology
Earth and Planetary Science Letters, 36 (1977), pp. 359–362

Sun et al., 2004
T. Sun, X.M. Zhou, P.R. Chen, H.M. Li, H.Y. Zhou, Z.C. Wang, W.Z. Shen
Strongly peraluminous granites of Mesozoic in eastern Nanling Range, Southern China: petrogenesis and implications for tectonics
Science in China (Series D), 48 (2004), pp. 165–174

Sun et al., 2011
Y. Sun, C.Q. Ma, Y.Y. Liu, Z.B. She
Geochronological and geochemical constraints on the petrogenesis of late Triassic aluminous *A*-type granites in southeast China
Journal of Asian Earth Sciences, 42 (2011), pp. 1117–1131

Suo et al., 1999
S.T. Suo, X.H. Bi, H.W. Zhou
Very Low Grade Metamorphism
Geological Publishing House, Beijing (1999) pp. 1–68

Tan et al., 2008
J. Tan, J.H. Wei, S.R. Li
Geochemical characteristics and tectonic significance of Kunlunguan *A*-type granite, Guangxi
Earth Science-Journal of China University of Geosciences, 33 (2008), pp. 743–754

Tapponnier et al., 1990
P. Tapponnier, R. Lacassin, H. Lelaup, U. Scharer, D.L. Zhong, H.W. Wu, X.H. Liu, S.C. Ji, L.S. Zhang, J.Y. Zong
The Ailao Shan/Red River metamorphic belt: tertiary left-lateral shear between Indochina and South China
Nature, 342 (1990), pp. 431–437

Tran and Halpin, 2011
Tran, Hai Thanh, Halpin, J., 2011. Structural features of magamatic complexes in Ngan Son area, Bac Kan province and their significance in regional tectonic framework. International Workshop on Advanced Research in Geosciences in Asia, Hanoi.

Tran et al., 2008
T.H. Tran, A.E. Izokh, G.V. Polyakov, A.S. Borisenko, T.A. Tran, P.A. Balykin, T.P. Ngo, S.N. Rudnev, V.V. Vu, A.N. Bui
Permo-Triassic magmatism and metallogeny of Northern Vietnam in relation to the Emeishan plume
Russian Geology and Geophysics, 49 (2008), pp. 480–491

Valley et al., 1998
J.W. Valley, P.D. Kinny, D.J. Schulze, M.J. Spicuzza
Zircon megacrysts from kimberlite: oxygen isotope variability among mantle melts
Contributions to Mineralogy and Petrology, 133 (1998), pp. 1–11

Valley et al., 2005
J.W. Valley, J.S. Lackey, A.J. Cavosie, C.C. Clechenko, M.J. Spicuzza, M.A.S. Basei, I.N. Bindeman, V.P. Ferreira, A.N. Sial, E.M. King, W.H. Peck, A.K. Sinha, C.S. Wei
4.4 billion Years of crustal maturation: oxygen isotope ratios of magmatic zircon
Contributions to Mineralogy and Petrology, 150 (2005), pp. 561–580

Van Tri, 1979

Van Tri
Geology of Vietnam: The Northern Part
Science and Technique Publishing House, Hanoi (1979) pp. 80

Wan et al., 2010
Y.S. Wan, D.Y. Liu, S.M. Wilde, J.J. Cao, B. Chen, C.Y. Dong, B. Song, L.L. Du
Evolution of the Yunkai Terrane, South China: evidence from SHRIMP zircon U–Pb dating, geochemistry and Nd isotope
Journal of Asian Earth Sciences, 37 (2010), pp. 140–153

Wang and Li, 2003
J. Wang, Z.X. Li
History of Neoproterozoic rift basins in South China: implications for Rodinia break-up
Precambrian Research, 122 (2003), pp. 141–158

Wang et al., 2000
X.F. Wang, I. Metcalfe, P. Jian, L.Q. He, C.S. Wang
The Jinshajiang-Ailaoshan Suture Zone, China: tectonostratigraphy, age and evolution
Journal of Asian Earth Sciences, 18 (2000), pp. 675–690

Wang et al., 2001
D.Z. Wang, L.S. Shu, M. Faure, W.Z. Shen
Mesozoic magmatism and granitic dome in the Wugongshan massif, Jiangxi Province and their genetical relationship to the tectonic events in southeast China
Tectonophysics, 339 (2001), pp. 259–277

Wang et al., 2002
Y.J. Wang, Y. Zhang, W.M. Fan, X.W. Xi, F. Guo, G. Lin
Numerical modeling of the formation of Indosinian peraluminous granitoids in Hunan Province: basaltic underplating versus tectonic thickening
Science in China (Series D), 11 (2002), pp. 491–499

Wang et al., 2005
Q. Wang, J.W. Li, P. Jian, Z.H. Zhao, X.L. Xiong, Z.W. Bao, J.F. Xu, C.F. Li, J.L. Ma
Alkaline syenites in eastern Cathaysia (South China): link to Permian-Triassic transtension
Earth and Planetary Science Letters, 230 (2005), pp. 339–354

Wang et al., 2007a
Wang, Y.J., Fan, W.M., Cawood, P.A., Ji, S.C., Peng, T.P., Chen, X.Y., 2007a. Indosinian high-strain deformation for the Yunkaidashan tectonic belt, South China: Kinematics and $^{40}Ar/^{39}Ar$ geochronological constraints. Tectonics 26, TC6008, doi: 10.1029/2007TC002099.

Wang et al., 2007b
Y.J. Wang, W.M. Fan, M. Sun, X.Q. Liang, Y.H. Zhang, T.P. Peng

Geochronological, geochemical and geothermal constraints on petrogenesis of the Indosinian peraluminous granites in the South China Block: a case study in the Hunan Province
Lithos, 96 (2007), pp. 475–502

Wang et al., 2007c
Y.J. Wang, W.M. Fan, G.C. Zhao, S.C. Ji, T.P. Peng
Zircon U–Pb geochronology of gneissic rocks in the Yunkai massif and its implications on the Caledonian event in the South China Block
Gondwana Research, 12 (2007), pp. 404–416

Wang et al., 2010
Wang, Y.J., Zhang, F.F., Fan, W.M., Zhang, G.W., Chen, S.Y., 2010. Tectonic setting of the South China Block in the early Paleozoic: Resolving intracontinental and ocean closure models from detrital zircon U–Pb geochronology. Tectonics 29, TC6020, doi: 10.1029/2010TC002750, 2010.

Wang et al., 2011
Y.J. Wang, A.M. Zhang, W.M. Fan, G.W. Zhang, F.F. Zhang, Y.Z. Zhang, S.Z. Li
Kwangsian crustal anatexis within the eastern South China Block: geochemical, zircon U–Pb geochronological and Hf isotopic fingerprints from the gneissoid granites of Wugong and Wuyi-Yunkai
Lithos, 127 (2011), pp. 239–260

Wang et al., 2012a
Y. Wang, W. Fan, G. Zhang, Y. Zhang
Phanerozoic tectonics of the South China Block: key observations and controversies
Gondwana Research (2012) http://dx.doi.org/10.1016/j.gr.2012.02.019

Wang et al., 2012b
Y.J. Wang, C.M. Wu, A.M. Zhang, W.M. Fan, Y.H. Zhang, Y.Z. Zhang, T.P. Peng, C.Q. Yin
Kwangsian and Indosinian reworking of the eastern South China Block: constraints on zircon U–Pb geochronology and metamorphism of amphibolites and granulites
Lithos, 150 (2012), pp. 227–242

Wei et al., this volume
Wei, W., Chen, Y., Faure, M., Shi, Y.H., Martelet, G., Huo, Q.L., Lin, W., Le Breton, N., Wang, Q.C., this volume. A multidisciplinary study on the emplacement mechanism of the Qingyang-Jiuhua Massif in Southeast China and its tectonic bearings. Part I: structural geology, AMS and paleomagnetism. Journal of Asian Earth Sciences, in press.

Wiedenbeck et al., 1995
M. Wiedenbeck, P. Alle, F. Corfu, W.L. Griffin, M. Meier, F. Oberli, A. Vonquadt, J.C. Roddick, W. Speigel
Three natural zircon standards for U–Th–Pb, Lu–Hf, trace-element and REE analyses

Geostandards Newsletter, 19 (1995), pp. 1–23

Wiedenbeck et al., 2004
M. Wiedenbeck, J.M. Hanchar, W.H. Peck, P. Sylvester, J. Valley, M. Whitehouse, A. Kronz, Y. Morishita, L. Nasdala, J. Fiebig, I. Franchi, J.P. Girard, R.C. Greenwood, R. Hinton, N. Kita, P.R.D. Mason, M. Norman, M. Ogasawara, P.M. Piccoli, D. Rhede, H. Satoh, D. Schulz-Dobrik, O. Skar, M.J. Spicuzza, K. Terada, A. Tindle, S. Togashi, T. Vennemann, Q. Xie, Y.F. Zheng
Further characterization of the 91,500 zircon crystal
Geostand Geoanalytical Research, 28 (2004), pp. 9–39

Wu et al., 2006a
F.Y. Wu, Y.H. Yang, L.W. Xie, J.H. Yang, P. Xu
Hf isotopic compositions of the standard zircons and baddeleyites used in U–Pb geochronology
Chemical Geology, 234 (2006), pp. 105–126

Wu et al., 2006b
R. Wu, Y. Zheng, Y. Wu, Z. Zhao, S. Zhang, X. Liu, F. Wu
Reworking of juvenile crust: element and isotope evidence from Neoproterozoic granodiorite in south China
Precambrian Research, 146 (2006), pp. 179–212

Xie et al., 2006
C.F. Xie, J.C. Zhu, S.J. Ding, Y.M. Zhang, M.L. Chen, Y.R. Fu, T.A. Fu, Z.H. Li
Age and petrogenesis of the Jianfengling granite and its relationship to metallogenesis of the Baolun gold deposit, Hainan Island
Acta Petrologica Sinica, 22 (2006), pp. 2493–2508

Xu et al., 1987
J. Xu, G. Zhu, W. Tong, K. Cui, Q. Liu
Formation and evolution of the Tancheng-Lujiang wrench fault system: a major shear system to the northwest Pacific Ocean
Tectonophysics, 134 (1987), pp. 273–310

Xu et al., 2001
Y.G. Xu, S.L. Chung, B.M. Jahn, G.Y. Wu
Petrologic and geochemical constraints on the petrogenesis of Permian-Triassic Emeishan flood basalts in southwestern China
Lithos, 58 (2001), pp. 145–168

Xu et al., 2004
Y.G. Xu, B. He, S.L. Chung, M.A. Menzies, F.A. Frey
Geologic, geochemical, and geophysical consequences of plume involvement in the Emeishan flood-basalt province
Geology, 10 (2004), pp. 917–920

Yan et al., 2003
D.P. Yan, M.F. Zhou, H.L. Song, X.W. Wang, J. Malpas
Origin and tectonic significance of a Mesozoic multi-layer over-thrust system within the Yangtze block (south China)

Tectonophysics, 361 (2003), pp. 239–254

Yan et al., 2005
D.P. Yan, M.F. Zhou, Y. Wang, C.L. Wang, T.P. Zhao
Structural styles and chronological evidences from Dulong-Song Chay tectonic dome: earlier spreading of south China sea basin due to late mesozoic to early cenozoic extension of south China block
Earth Science-Journal of China University of Geosciences, 30 (2005), pp. 402–412

Yan et al., 2006
D.P. Yan, M.F. Zhou, C.Y. Wang, B. Xia
Structural and geochronological constraints on the tectonic evolution of the Dulong-Song Chay tectonic dome in Yunnan province, SW China
Journal of Asian Earth Sciences, 208 (2006), pp. 332–353

Yan et al., 2011
D.P. Yan, M.F. Zhou, S.B. Li, G.Q. Wei
Structural and geochronological constraints on the Mesozoic-Cenozoic tectonic evolution of the Longmen Shan thrust belt, eastern Tibetan Plateau
Tectonics, 30 (2011), p. TC6005 doi: 10.1029/2011TC002867.

Yang and Besse, 1993
Z. Yang, J. Besse
Paleomagnetic study on Permian and Mesozoic sedimentary rocks from North Thailand supports the extrusion model for Indochina
Earth and Planetary Science Letters, 117 (1993), pp. 525–552

Yu et al., 2006
J. Yu, W. Shen, L. Wang, L. Shu, T. Sun
Cathaysia block: a young continent composed of ancient materials
Geological Journal of China Universities, 12 (2006), pp. 440–447

Yu et al., 2007
J. Yu, Y.S. O Reilly, L. Wang, W.L. Griffin, S. Jiang, Y. Wang, X. Xu
Finding of ancient materials in Cathaysia and implication for the formation of Precambrian crust
Chinese Science Bulletin, 52 (2007), pp. 11–18

ZBGMR, 1989
ZBGMR (Zhejiang Bureau of Geology and Mineral Resources), 1989. Regional Geology of Zhejiang Zejian Province. Geological Publishing House, Beijing, pp. 688.

Zhang et al., 1984
Z.M. Zhang, J.G. Liou, R.G. Coleman
An outline of the plate tectonics of China
Geologyical Society of America Bulletin, 95 (1984), pp. 295–312

Zhang et al., 2008

X.H. Zhang, H.F. Zhang, Y.J. Tang, S.A. Wilde, Z.C. Hu
Geochemistry of Permian bimodal volcanic rocks from Central Inner Mongolia, North China: implication for Tectonic setting and Phanerozoic continental growth in Central Asian Orogenic Belt
Chemical Geology, 249 (2008), pp. 262–281

Zhang et al., 2011
F.F. Zhang, Y.J. Wang, X.Y. Chen, W.M. Fan, Y.H. Zhang, A.M. Zhang
Triassic high-strain shear zones in Hainan Island (South China) and their implications on the amalgamation of the Indochina and South China Blocks: Kinematic and $^{40}Ar/^{39}Ar$ geochronological constraints
Gondwana Research, 19 (2011), pp. 910–925

Zhao et al., 2010
L. Zhao, F. Guo, W.M. Fan, C.W. Li, X.F. Qin, H.X. Li
Crustal evolution of the Shiwandashan area in South China: Zircon U–Pb–Hf isotopic records from granulite enclaves in Indo-Sinian granites
Chinese Science Bulletin, 55 (2010), pp. 2028–2038

Zhou and Li, 2000
X.M. Zhou, W.X. Li
Origin of Late Mesozoic igneous rocks in Southeastern China: implications for lithosphere subduction and underplating of mafic magmas
Tectonophysics, 326 (2000), pp. 269–287

Zhou and Zhu, 1993
X.M. Zhou, Y.H. Zhu
Petrologic data from the Late Proterozoic collision-orogenic belt and suture zone in the southeast of China
J.L. Li (Ed.), Crustal Structure and Geological Evolution of Southeast Continents, Publishing House of Metallurgy and Industry, Beijing (1993), pp. 87–97

Zhou et al., 2006
X. Zhou, T. Sun, W. Shen, L. Shu, Y. Niu
Petrogenesis of Mezozoic granitoids and volcanic rocks in south China: a response to tectonic evolution
Episodes, 29 (2006), pp. 26–33